DOCTORAL DISSERTATION SERIES
Publication No.: 11,377

AUTHOR: Karl Dawson Wood, Ph. D., 1955
University of Michigan

TITLE: AERODYNAMIC DESIGN OF HELICOPTERS

University Microfilms, Ann Arbor, Michigan

AERODYNAMIC DESIGN OF HELICOPTERS

by

Karl Dawson Wood

A dissertation submitted in partial fulfillment
of the requirements for the degree of
Doctor of Philosophy in the
University of Michigan
1955

Committee in charge:

Professor Wilbur C. Nelson, Chairman
Professor Arnold M. Kuethe
Associate Professor Edgar J. Lesher
Professor Jesse Ormondroyd
Professor J. D. Schetzer
Mr. Joseph Stuart III, Chief of Preliminary Design,
Hiller Helicopters, Palo Alto, California

Abstract of Ph. D. Dissertation

AERODYNAMIC DESIGN OF HELICOPTERS

By Karl Dawson Wood

An integrated series of helicopter performance charts is developed covering hovering, level flight, climb, glide, and landing without power.

The method used is a mathematical synthesis of theoretical equations with empirical coefficients to put the desired results in a form readily usable by engineers in making design compromises.

The assumptions involved in the theoretical equations are reviewed; only widely accepted assumptions and equations are involved.

Two basic series of charts are involved: 1) two new types of hovering power charts, and 2) a novel series of general charts for power required for level flight.

The hovering power charts permit quick estimates to be made of the hovering power required as a function of various parameters, including solidity, disc loading, and tip speed with specified limits on retreating blade stall and advancing blade shock wave loss, and indicate the areas in which power-off landings may be hazardous.

The level flight charts consist of 1) a series of general charts of power required for level flight, expressed in terms of hovering power, and 2) charts for level high speed and climb or glide as a function of the appropriate parameters.

The charts are considered to be correct with engineering accuracy (plus or minus five per cent) for the configurations for which they are plotted. Two ranges of blade drag coefficient are considered, corresponding to typical two-blade and three-blade single-rotor configuration. Correction factors for multi-rotor configurations are discussed.

The methods and results of this dissertation are consistent with current design practice, and the charts here developed are shown by illustrative examples to facilitate the repeated trials and compromises necessary in evolving an economical helicopter design.

PREFACE

The following study was undertaken for the purpose of providing engineers and students in aeronautical engineering with a simple procedure for preliminary design of a helicopter for a specified payload and performance. The principal requirement of an acceptable procedure is considered to be that the resulting design, if constructed and flown, would perform in flight very nearly as calculated.

An illustrative example of design procedure is provided. The procedure here described has been evolving over a period of about two years, and has been used by students in developing new helicopter designs; major revisions in the procedure have been made for better coordination with established theory as a result of specific criticisms by members of the committee.

The major contribution of this dissertation to the art of helicopter design is the development of an integrated series of performance charts covering hovering, level flight, climb, glide, and landing without power. The resulting design charts are believed to be not only consistent with accepted theory but also novel in the following respects.

(1) A quantitative general power requirement chart for level flight of helicopters has been developed. No such chart has previously been published in the literature available to the author of this dissertation. Such a chart is shown to be very useful, and is in fact

what makes a simple design procedure possible.

(2) Speed limitations due to advancing blade shock and retreating blade stall have been put in such form that they can be represented on a hovering design chart and considered at the same time that hovering performance is being considered.

(3) The conditions necessary for a helicopter to land completely without shock from a descent without power are also represented on the hovering design chart.

The methods and results of this dissertation are shown to be consistent with current design practice and the charts here developed are shown to facilitate the repeated trial calculations necessary in evolving the most economical design for a given payload and performance.

Particular thanks are due to Mr. Joseph Stuart III for his many suggestions in bringing this presentation in line with accepted practice.

TABLE OF CONTENTS

CHAPTER		PAGE
	PREFACE	ii
	LIST OF FIGURES	v
	NOTATION	vii
I	PHYSICAL BACKGROUND OF THE PROBLEM	1
II	HOVERING ROTOR THEORY AND COMPARISON WITH TEST DATA	9
III	SPEED LIMITATIONS	22
IV	BLADE LIFT COEFFICIENTS FOR HOVERING POWER CHART	28
V	USE OF HOVERING POWER CHARTS	31
VI	HELICOPTER THEORY IN FORWARD FLIGHT	35
VII	CHECK ON TEST DATA IN FORWARD FLIGHT	40
VIII	CHARTS FOR CLIMB AND LEVEL HIGH SPEED	43
IX	SINKING SPEED WITHOUT POWER	45
X	LANDING WITHOUT POWER	50
XI	WEIGHT ANALYSIS OF HELICOPTERS	54
XII	DESIGN TO A PERFORMANCE SPECIFICATION	60
XIII	CONCLUDING REMARKS	63
	REFERENCES	64
	FIGURES 5 TO 23, INCLUSIVE	66 TO 84

LIST OF FIGURES

FIGURE		PAGE
1.	Sketches of Helicopters Showing Arrangements Considered. . .	2
2.	Two Types of Pitch Control Mechanism.	4
3.	Changes in Air Velocity, Blade Forces, and Blade Position with Azimuth Position Around Cycle in Forward Flight . . .	6
4.	Blade Element and Result of Integrating Blade Element Forces on Power Required for Level Flight	8
5.	Helicopter Tower Test Data Fitted by Family of Straight Lines of Form $10^5 C_{Q_o} = 10^5 C_{Q_o} + k(1000 C_T)^{3/2}$, with k = 2.7	66
6.	Intercepts C_{Q_o} from Figure 5 Plotted Against σ	67
7.	Hovering Power Chart Based on Three-Blade Tower Test Data. .	68
8.	Rotor Figure of Merit for Bell and Seibel Helicopters. . . .	69
9.	Reciprocal Figure of Merit Plotted vs. $(\sigma/2C_T)^{3/2}$ for Comparison of Flight Tests and Theory.	70
10.	Summary of Retreating Blade Stall Limitations.	71
11.	Plot of Retreating Blade Stall Limitations Based on Figure 10	72
12.	Hovering Power per 1000 Pounds Gross Weight Plotted vs. V_t with w and σ as Parameters for a Constant Rotor Limit of $mph_{LS} = 100$.	73
13.	Hovering Power Chart for Two-blade Helicopters Based on Flight Test Data in Figure 9	74
14.	Variation of Induced and (Profile + Body) Power with Speed Ratio	75

FIGURE PAGE

15. General Power Required Chart for Level Flight of Optimum Helicopters ($r_h = p_{hp}/p_{hp} = 2$) 76

16. General Power Required Chart for $r_h = 1$. 77

17. General Power Required Chart for $r_h = 3$. 78

18. General Power Required Chart for $r_h = 5$. 79

19. Flight Test Check on General Power Required Chart. 80

20. Sea Level High Speed Chart for Optimum Designed Helicopters with $r_h = 2$ 81

21. Maximum Sea Level Climb Chart for Optimum Designed Helicopters with $r_h = p_{hi}/p_{hp} = 2$. 82

22. Simplified Approximate Calculated Sinking Speed of Helicopters in Autorotative Descent at the Rotative Speeds Specified Above 83

23. Plot of Some Rotor Blade Weights, Based on Data in Reference 1 84

NOTATION

Most of the notation used in this dissertation follows current practice of the National Advisory Committee for Aeronautics, which practice is also followed by most of the references. The few departures from current practice are considered justified in the interest of simplifying the appearance of the particular equations involved in this dissertation. The arrangement of symbols is alphabetical, first English, then Greek.

English Notation

a	speed of sound (feet per second); also lift curve slope.
A	area (square feet), usually propeller disc area. $A = \pi R^2$
AR_e	aspect ratio of outer half of a blade. $AR_e = R/2c_e$
b	number of blades
B	blade tip loss factor
Bhp	brake horsepower. $Bhp = P/550$
c	chord at any point on blade (feet)
c_d	blade section drag coefficient
c_{de}	mean effective blade section drag coefficient
c_e	mean effective blade chord (feet). $c_e = \dfrac{\int_o^R cr^2 dr}{\int_o^R r^2 dr}$
c_l	blade section lift coefficient
C_h	rate of climb (feet per minute)
C_L	rotor lift coefficient

English Notation, (Continued)

$\bar{C}_{Lb}$ mean blade lift coefficient

C_Q rotor torque coefficient. $C_Q = \frac{Q}{\rho \pi R^3 (\Omega R)^2} = \frac{P}{\rho A V_t^3}$

C_T rotor thrust coefficient. $C_T = \frac{T}{\rho \pi R^2 (\Omega R)^2} \quad \frac{T}{\rho A V_t^2}$

D rotor diameter (feet)

f flat plate area (square feet) of unity drag coefficient equivalent to the body (or parasite) drag

f( ) function of

f* body drag factor. $f^* = \frac{4 f}{c_{de} A \sigma}$

F_m figure of merit

g acceleration of gravity (32.2 feet per second per second)

h height or altitude (feet)

I moment of inertia (slug-feet^2)

k a constant; slope of graph of $10^5 C_Q$ versus $1000 C_T$; radius of gyration (feet).

k_h ratio of actual to ideal induced power in hovering

L lift (pounds)

mph miles per hour

M Mach Number

M_{fs} free stream Mach Number

p rotor horsepower per 1000 pounds gross weight (numerous subscripts for p designated below)

P rotor power (foot-pounds per second), (numerous subscripts for P designated below).

English Notation, (Continued)

P/L sum of D/L values for helicopter, defined on page 22.

Q rotor torque (pound-feet).

r radius from rotor axis to any point on blade (feet).

r_h ratio of hovering induced to hovering profile power. $r_h = \frac{P_{hi}}{P_{hp}}$

R rotor radius (feet).

R* ratio of power in forward flight to hovering power.

R_i ratio of induced power in forward flight to induced hovering power.

R_p ratio of (profile plus body) power in forward flight to profile hovering power.

s span of wing.

S surface area (square feet).

t rotor blade thickness (feet).

T rotor thrust (pounds). For steady flight, nearly level, T = W.

v rotor tip speed in hundreds of feet per second. $v = V_t/100$

V velocity (feet per second), (velocity of level flight without subscript; numerous subscripts designated below)

w disc loading corrected to sea level (pounds per square foot). $w = \frac{W}{A}\frac{\rho_o}{\rho}$

W gross weight of helicopter (pounds), (numerous subscripts for component weights designated below).

x non-dimensional blade stations, measured from rotor axis. $x = r/R$

Summary of Subscripts

$( )_b$	body (or parasite) or blade
$( )_c$	climb or compressibility
$( )_{deg}$	degrees
$( )_e$	effective
$( )_{emp}$	empty
$( )_{eng}$	engine
$( )_g$	gears
$( )_{gb}$	bevel gears
$( )_{gp}$	planetary gears
$( )_h$	hovering
$( )_i$	induced
$( )_{id}$	ideal
$( )_l$	lift
$( )_{LS}$	limited by stall
$( )_{LSc}$	limited by stall and compressibility
$( )_{max}$	maximum
$( )_o$	sea level; sometimes profile (for wing sections).
$( )_p$	profile
$( )_{pl}$	pay load
$( )_{pp}$	power plant
$( )_r$	rotor
$( )_{simp}$	simplified
$( )_s$	sinking
$( )_S$	stall
$( )_t$	tip

Summary of Subscripts, (Continued)

$( )_{trans}$	transmission
$( )_{v}$	vertical
$( )_{1, 2, 3, \text{etc.}}$	locations at points 1, 2, 3, etc.

Greek Notation

α	(alpha)	angle of attack (radians if not specified as degrees)
γ	(gamma)	tilt of thrust vector relative to line of flight
η	(eta)	efficiency
θ	(theta)	usually pitch angle from zero lift chord to plane normal to rotor axis
λ	(lambda)	inflow ratio, usually ratio of axial flow velocity at disc to tip speed
μ	(mu)	ratio of flight velocity along path to tip speed
π	(pi)	3.1416
ρ	(rho)	air density at any altitude (slugs per cubic foot)
ρ_o		air density at sea level (slugs per cubic foot)
σ	(sigma)	rotor solidity ratio; ratio of effective blade area to rotor disc area. $\sigma = \frac{bc_e}{\pi R} = \frac{bc_e R}{A}$
φ	(phi)	inflow angle (radians if not specified as degrees)
ψ	(psi)	azimuth angle of blade position, measured from blade downwind position (usually degrees; advancing blade angles 0 to 180°; retreating blade angles 180° to 360°)
Ω	(omega)	angular velocity of rotor (radians per second)

CHAPTER I

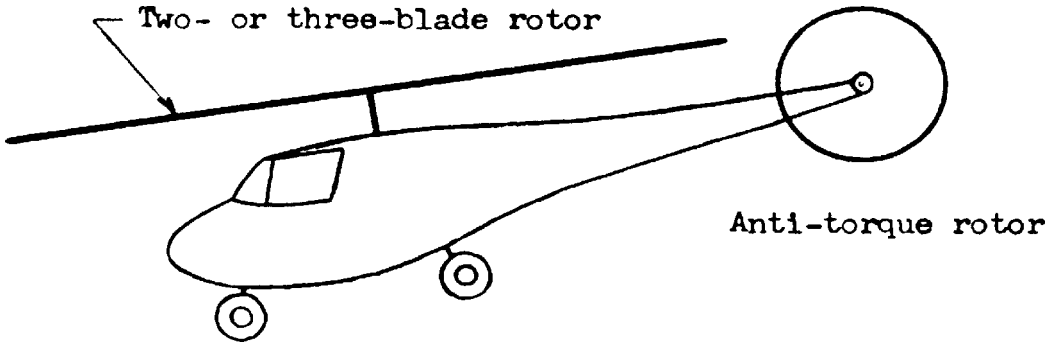
PHYSICAL BACKGROUND OF THE PROBLEM

The helicopter is a vehicle of ancient lineage, only recently become of considerable military and commercial importance with the satisfactory solution of the control problem. The dominant type has become the single rotor machine with anti-torque rotor shown in Figure 1(a), with the tandem-rotor machine of Figure 1(b) next, but used only for very heavy loads.

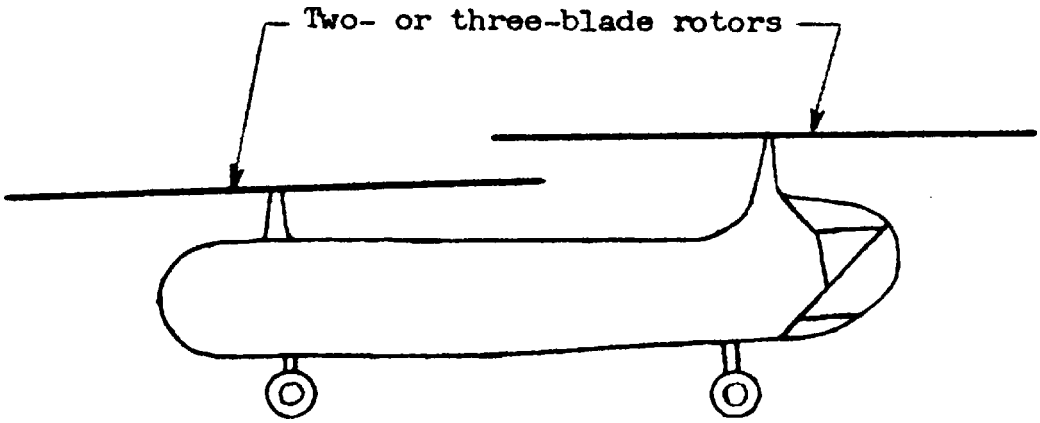
(a) Description of Helicopters and Their Operation.

A helicopter consists essentially of a body which encloses the payload and power plant, a rotor or rotors which provide lift by action similar to that of an airplane propeller, and a control system. The control system for a helicopter of the type of Figure 1(a) consists of a controllable pitch anti-torque rotor for control about the vertical axis, and a cyclic pitch control for the main rotor blades for control about the other two axes. The rotor blades must also have a collective pitch control to permit either vertical climb, hovering, or safe descent without power.

The pitch control mechanisms, which have made safe helicopter flight possible, are complicated and expensive; they are also heavy because they must be designed to fatigue limits much lower than yield stresses; they are also troublesome because they introduce vibration problems. Common types of pitch control mechanism are sketched in Figure 2. Vertical flight involves only the collective pitch control.



(a) Single-rotor with Anti-torque Rotor.

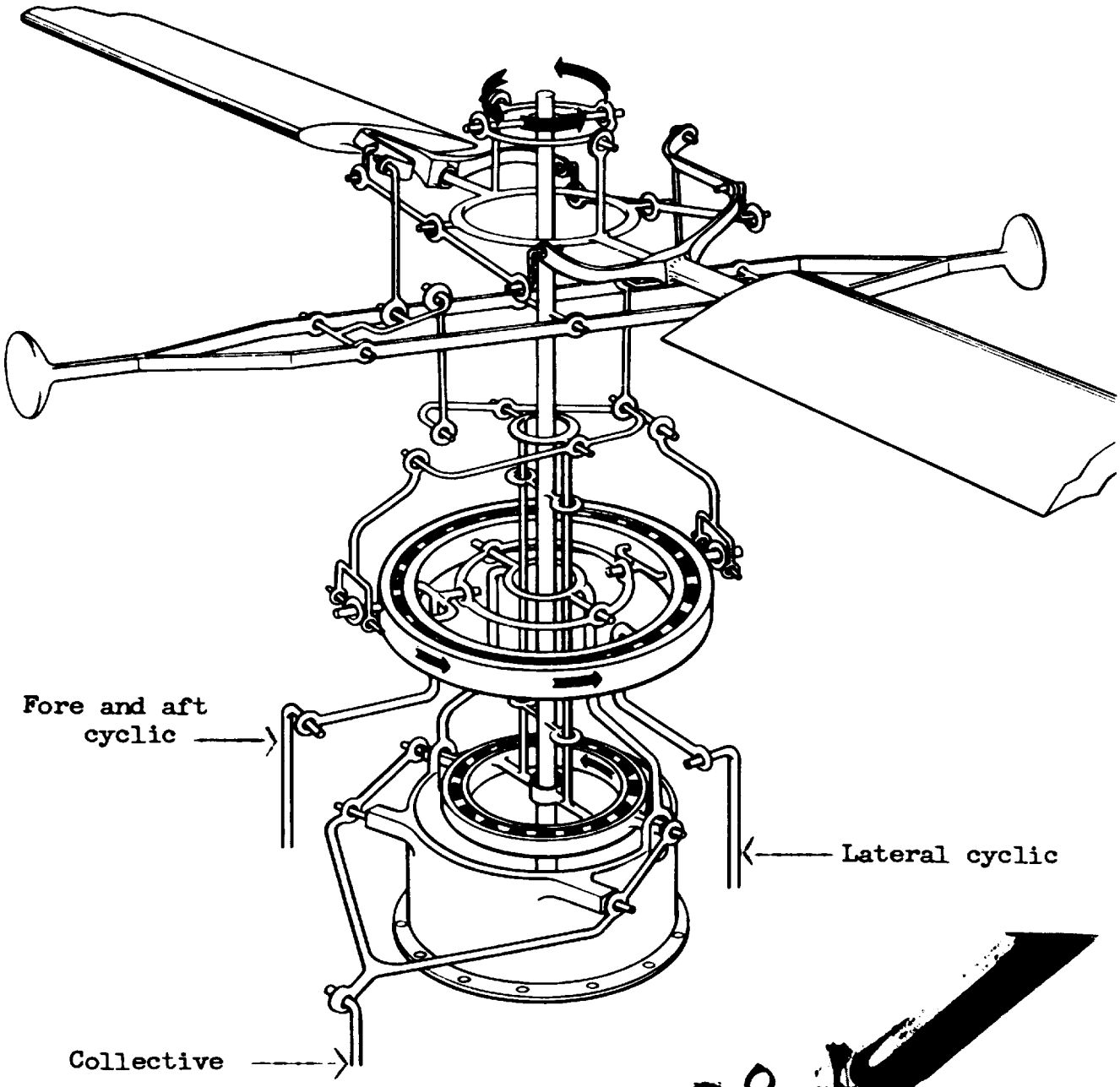


(b) Tandem Rotors.

Figure 1. Sketches of Helicopters Showing Arrangements Considered.

In horizontal or nearly horizontal flight, the pitch of each blade must be low when advancing, high when retreating, because the relative air velocity over the blades is approximately as shown in Fig. 3(a). With an idealized cyclic pitch control mechanism, in which the blade pitch varied not only with azimuth position but also varied cyclically along the blade radius, it would be possible for the lift vector on each blade [Figure 3(b)] to remain the same throughout the cycle of azimuth positions. With the practical mechanisms shown in Figure 2, however, the lift distribution will vary considerably throughout the cycle. The total lift per blade will also vary somewhat during the start of horizontal flight. The usual control operation in starting horizontal flight as explained in Reference 3, pages 162-169, is to set the cyclic pitch control so as to tilt the rotor disc forward. As forward velocity is picked up, there is increased lift on the advancing blade and decreased lift on the retreating blade. The resulting blade motion (flapping), sketched in Figure 3(c), then tilts the rotor tip path plane back and the flapping is considered in Reference 3 to impart a cyclic pitch variation (feathering) to the blades which tends to equalize the lifts of the advancing and retreating blades as steady forward flight develops.

If the retreating blade is to maintain a lift nearly equal to that of the advancing blade, it must operate at a much higher angle of attack and stall of the retreating blade limits the speed of forward flight. Angle of attack variations with azimuth position have been measured with good accuracy and are presented in Reference 3 (pages 251-253); lift variations are in some doubt, but it is often assumed, on the basis of moving picture observations of blade motions relative to the



(a) (Above) Bell Two-blade Mechanism.

(b) (Right) Sikorsky Three-blade Mechanism.

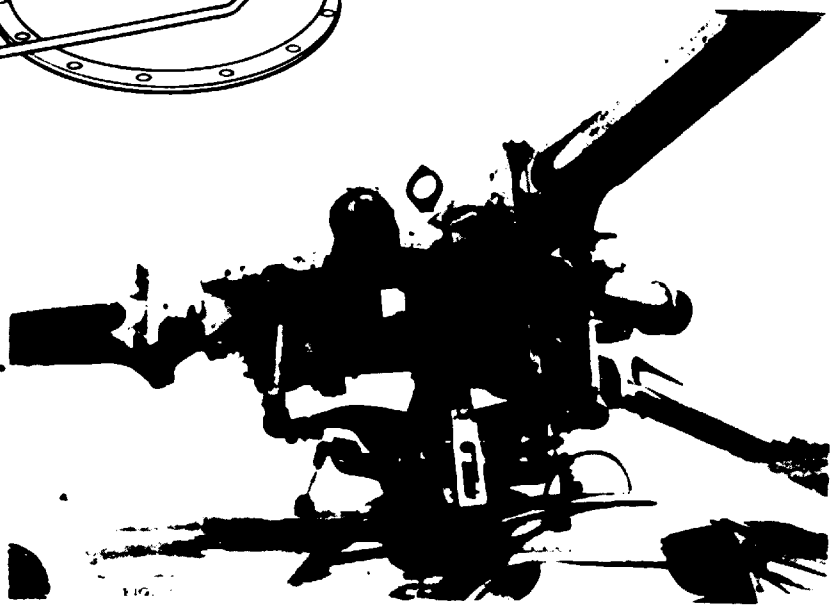


Figure 2. Two Types of Pitch Control Mechanism.

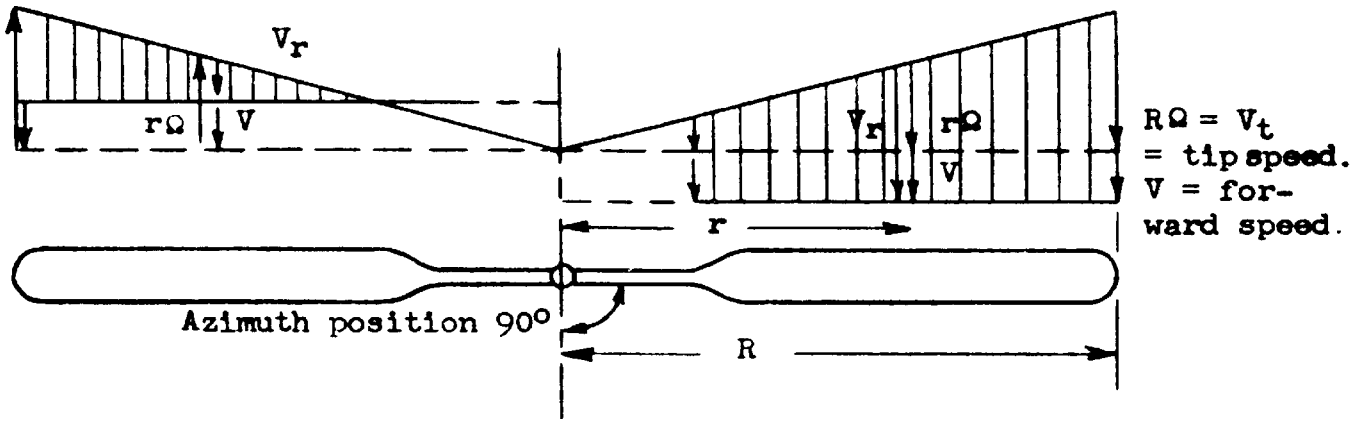
rotor tip plane that lift variations are small, except for higher harmonics of blade vibration.

(b) Outline of the Performance Calculation Problem.

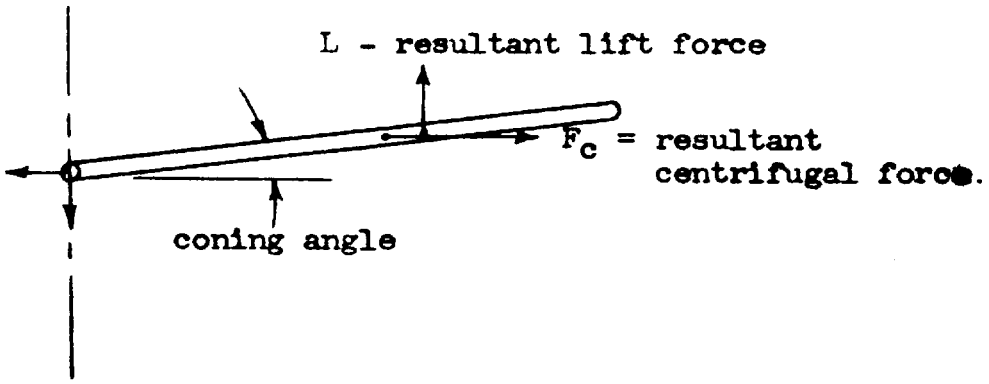
The problem with which this dissertation is chiefly concerned is the development of simplified methods for calculating rapidly and accurately the level flight performance of single-rotor helicopters such as that shown in Figure 1(a). Estimates are also made for applying these methods to tandem-rotor configurations like Figure 1(b). It is found convenient to use the hovering performance as a point of reference, and to extend the level flight performance calculations to include shallow climbs and glides. The theoretical treatment is an extension of airplane propeller theory, but since the assumptions of the theory are only very approximately fulfilled, the resulting equations require empirical coefficients to be applicable with good accuracy to the helicopter performance problem.

Hovering performance equations are here based on plots of flight test and full scale static thrust tests run on the static thrust test facility of the National Advisory Committee for Aeronautics, known as the test tower, because the rotor is mounted high above the ground to minimize the effect of proximity to the ground. A mathematical framework for plotting hovering flight and tower test measurements is provided by integrating the forces on blade elements such as that shown in Figure 4(a).

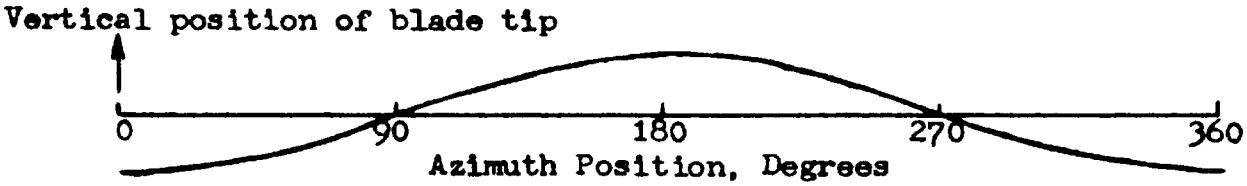
In forward flight, the velocity distribution along the blade shown in Figure 3(a), when integrated along the blade and around the



(a) Horizontal velocity distribution on blades of rotor in horizontal flight at $\mu = V/\Omega R \approx 1/3$.



(b) Free body sketch of an advancing blade, hinged to flap, with principal resultant forces shown, blade flexibility neglected. Drag forces are perpendicular to the plane of this view.

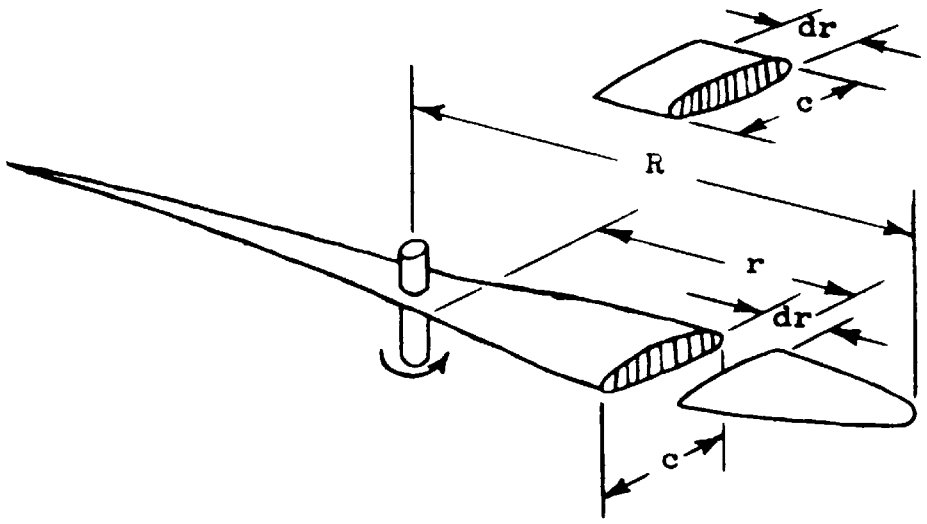


(c) Typical variation of vertical blade tip position (relative to plane normal to rotor axis) with azimuth position due to the usual cyclic pitch control action.

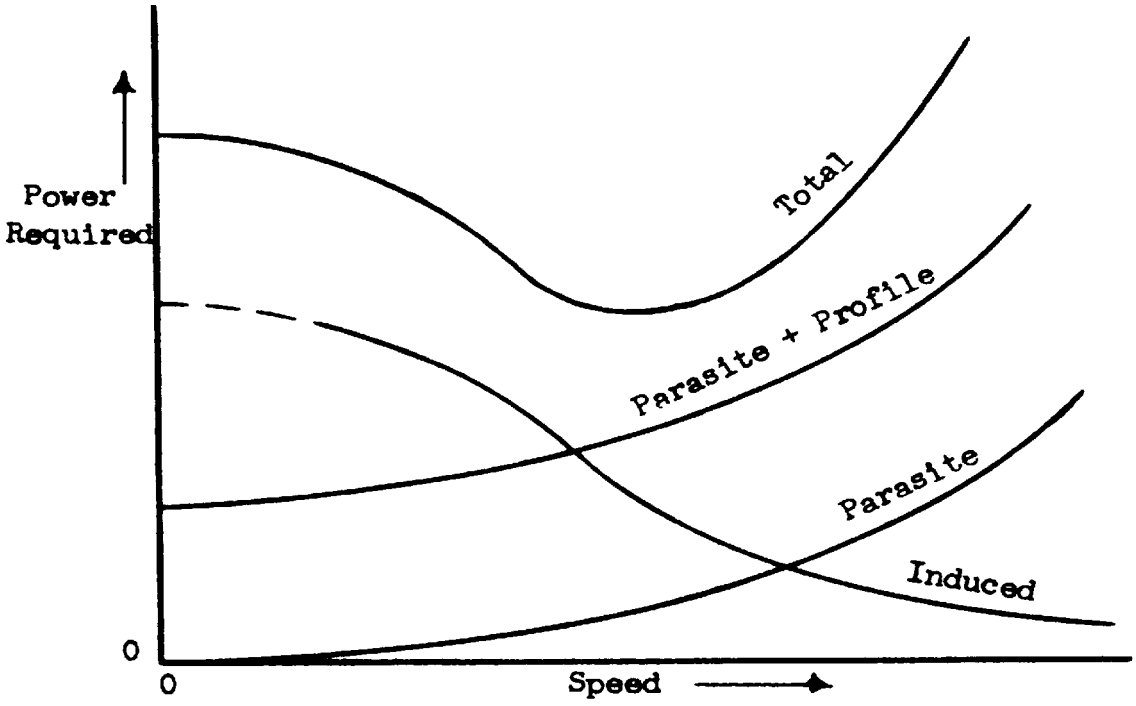
Figure 3. Changes in Air Velocity, Blade Forces, and Blade Position with Azimuth Position Around Cycle in Forward Flight.

azimuth, shows an increase in power required due to drag of the blade profile as forward speed is increased, as shown in Figure 4(b). The drag of the helicopter body, landing gear, and other exposed parts (profile drag) also increases with forward speeds as shown in Figure 4(b). There is, however, a reduction with forward speed of the power which must be supplied to the air stream flowing through the rotor disc, because the rotor disc operates on an increasing amount of air as forward speed is increased. This is called the "induced" power, and a typical variation with forward speed is also shown in Figure 4(b). The total power, which is the sum of parasite, profile, and induced power, thus reaches a minimum at some small forward speed. By calculating and plotting ratios of power required in forward flight to hovering power, a series of general graphs of power required against speed is obtained, and these graphs provide a basis for calculating level high speed and rate of climb on descent in the same manner as is customary for airplanes.

The resulting charts may be regarded as a helicopter version of the well known Oswald performance charts for airplanes, originally presented in NACA TR 408.



(a) Blade Element of Helicopter Rotor.



(b) Power Required as a Function of Forward Speed.

Figure 4. Blade Element and Result of Integrating Blade Element Forces on Power Required for Level Flight.

CHAPTER II

HOVERING ROTOR THEORY AND COMPARISON WITH TEST DATA

The following presentation of the assumptions and results of theoretical analysis of hovering rotors is a brief review of the literature in this field, and a criticism of the validity of some of the assumptions where experimental confirmation is available. This review is not intended to be original but is presented here as a critical review of the theory and for the purpose of minimizing consultation of references by the reader of this dissertation who may desire to follow the development of the mathematical relationships.

(a) Momentum Theory.

If a helicopter is climbing at a speed V_c, the air approaches the disc at this speed and at some distance below the disc has a higher speed equal to $V_c + v_1$, where v_1 represents the change of velocity on going through the disc. The mass of air per second flowing through the disc area is assumed to be $A\rho(V_c + v_i)$ where v_i is the increase in velocity at the disc and is later shown to be related to v_1. From Newton the thrust developed is

$$T = \rho A(V_c + v_i)v_1 \quad - \quad (1)$$

The thrust may also be considered to be equal to the disc area times the difference in pressure across the disc as indicated below:

$$T = A \Delta P \quad - \quad (2)$$

Writing Bernoulli's equation for the flow on either side of the disc, but not across it, and assuming that there is a change in pressure

but no change in velocity in going through the rotor disc, gives the result shown below:

$$\Delta P = \rho (V_c + \tfrac{1}{2}v_1)v_1 \quad - \quad (3)$$

Solving equations (1), (2) and (3) simultaneously permits showing that

$$v_i = \tfrac{1}{2}v_1 \quad - \quad (4)$$

For a hovering helicopter with $V_c = 0$ combination of equations (1) and (4) gives

$$T = 2A\rho v_i^2 \quad - \quad (5)$$

For steady (unaccelerated) hovering, T = W and the induced velocity at the disc is given by

$$v_i = \sqrt{\frac{W}{2A\rho}} \quad - \quad (6)$$

The ratio W/A is commonly referred to as the disc loading and designated by the symbol w, but it is preferred here to use w to designate the ratio $\frac{W}{A}\frac{\rho_o}{\rho}$ which will be called the corrected disc loading or disc loading corrected to sea level. Since $\rho_o = 1/420$,

$$v_i = \sqrt{\frac{1}{2\rho_o}}\sqrt{w} = 14.5\sqrt{w} \quad - - - - - - - - - - - - - - - \quad (7)$$

The power which must be supplied to the air to support the helicopter may be designated by p_{hi} and from the definition of power this is

$$p_{hi_{id}} = T\, v_i \quad - \quad (8)$$

the additional subscript id being used to designate an ideal value satisfying the assumptions of the momentum theory. Since it is usually convenient in engineering calculations to calculate power in horsepower and to refer to gross weights in thousands of pounds, or kips, it is convenient to have a special symbol for horsepower per thousand pounds

of gross weight and this is chosen as p, hence

$$P_{hi_{id}} = \frac{P_{hi}/550}{W/1000} = \frac{1000}{550}\sqrt{\frac{1}{2\rho_o}}\sqrt{W} = 26.4\sqrt{W} \quad \text{- - - - - - - - (9)}$$

Introducing the usual definitions $C_T = T/\rho AV_t^2$ and $C_Q = Q/\rho ARV_t^3 = P/\rho AV_t^3$, equation (9) may be written, for T = W

$$C_{Q_{i_{id}}} = \frac{1}{\sqrt{2}} C_T^{3/2} \quad \text{- (10)}$$

The ratio $C_T^{3/2}/C_{Q_{i_{id}}}$, which is seen in equation (10) to be $\sqrt{2}$, is sometimes called the "ideal figure of merit" ($F_{mi} = \sqrt{2}$); actual values of F_m are of course always less than the $\sqrt{2}$.

The foregoing analysis assumes in effect an infinite number of blades (an actuator disc) and provides no means of representing the drag forces on the blades or the power required to overcome them. Accordingly, it is customary to consider, in additional theory, that each blade consists of an infinite number of rotating infinitesmal airfoils acted on by lift and drag forces, and to calculate the contribution of these forces to thrust and torque.

(b) Blade Element Theory.

Considering a blade element of chord c and length dr acted on by an airstream of velocity Ωr, expressions for the lift and drag forces on an element, from the definitions of lift and drag coefficient are

$$dL = \tfrac{1}{2}\rho c_l(\Omega R)^2 c\,dr \quad \text{- (11)}$$

$$dD = \tfrac{1}{2}\rho c_{do}(\Omega R)^2 c\,dr \quad \text{- (12)}$$

Consider that the lift and drag forces act at an angle ϕ to the thrust

and torque directions where

$$\varphi \simeq \tan \varphi \simeq \sin \varphi \simeq \frac{v_i}{\Omega R} \quad - - - - - - - - - - - - - - - - - - \quad (13)$$

It follows that the elements of thrust and torque are given by the equations

$$dT = dL \cos\varphi = dD \sin\varphi \quad - \quad (14)$$

$$dQ = (dL \sin\varphi + dD \cos\varphi) r \quad - - - - - - - - - - - - - - - - - - - \quad (15)$$

Thrust and torque may be calculated by integrating equations (14) and (15) over the radius of the blade and multiplying by the number of blades. The usual procedure for this calculation is to calculate the local angle of attack $\alpha = \theta - v_i/\Omega R$, where θ is the local blade angle measured from the plane normal to the rotor axis, and v_i is the local downwash, and calculate $c_l = a_o \alpha$, where a_o is the infinite aspect ratio lift curve slope. Equations (11) and (15) then give an expression for dQ/dr. Since the local downwash is a function of the local lift coefficient, a solution by successive approximations is necessary, but numerically feasible as illustrated in reference 4. The thrust and torque are calculated by integrating numerically or graphically

$$T = \int_0^R \frac{dT}{dr} \, dr \quad - \quad (16)$$

$$Q = \int_0^R \frac{dQ}{dr} \, dr \quad - \quad (17)$$

For refined calculations the variation of blade profile drag coefficient c_{do} with radius station and angle of attack is also considered, but this variation is usually small and it is more common to assume a uniform mean effective profile drag coefficient c_{de}.

Algebraic integration is feasible for certain simplified cases; the case of an ideally twisted blade and uniform rotor chord c, for example, is solved in reference 3 (page 83) to give for zero vertical climb and c_{do} = uniform = c_{de}

$$C_Q = \frac{\sigma c_{de}}{8} + \frac{C_T^{3/2}}{B\sqrt{2}} \qquad (18)$$

where σ = solidity = $\frac{bc}{\pi R}$. The first term on the right hand side of equation (18) is the profile torque coefficient, here designated by C_{Q_o}. The second term is the induced torque coefficient C_{Q_i} and differs from equation (10) only by the insertion of the semi-empirical blade tip loss factor B.

Equation (18) states that if c_{de} and B are independent of C_T, C_Q should plot as a straight line when plotted against $C_T^{3/2}$. Experimental data plotted in Figure 5 show this to be true within the limits of experimental error. The slope of such graphs $d(C_T^{3/2})/dC_Q$ is seen in Figure 5 to be 1.17 $\pm$ 0.05, which differs from $\sqrt{2}$ by a factor 1.21 $\pm$ 0.05. From these experimental data it might erroneously be inferred that 1/B = 1.21 $\pm$ 0.05 or B = 0.827 $\pm$ 0.033, but in reference 3 (as well as most of the other references) it is preferred to define B in terms of theoretical calculations of blade tip loss, analogous to Glauert's wing tip loss factor (reference 9, Figure 2:29), and to use a different symbol to designate the relationship between the actual and ideal values of $dC_Q/d(C_T^{3/2})$. Reference 2 calls this factor k but it is preferred in this dissertation to use the symbol k_h (designating the hovering condition), leaving the symbol k for the more general case in which forward flight may also be involved. The symbol k_h, which for the test

data of Figure 1 equals 1.21 $\pm$ 0.05 thus takes account not only of tip losses, but also of all other factors which cause the actual $dC_Q/d(C_T^{3/2})$ to differ from the ideal. Such factors are a) variation of c_{do} with c_l [the last two terms of equation (36) on page 83 of reference 3], and b) non-uniform distribution of downwash (uniform distribution was assumed in the momentum theory). The factor k_h is thus analogous to the reciprocal of Oswald's "airplane efficiency factor" e as presented in reference 9, Chapter 3.

The factor B is more limited in scope. For example, reference 2 defines B as R_e/R, where R_e is the "effective blade radius" interpreted as "that radius which will produce thrust equal to that of the actual rotor, with the provision that the lift producing abilities are maintained up to $r = R_e$, where they suddenly disappear." Reference 3 defines B by the statement "blade elements outboard of the radius BR are assumed to have profile drag but no lift." Various theoretical expressions for B are presented and discussed in references 2 and 3, but values of B less than 0.95 are rarely obtained, a typical numerical value being 0.97 for typical current helicopter designs and operating conditions.

The factor k_h, which includes 1/B as well as other factors, is judged to be as accurately predictable as B for proposed new designs, and since the equations using k_h [e.g., reference 2, page 106, equation (13)] are much simpler than those involving B [e.g., reference 3, page 83, equation (36)], the factor B is not used in this dissertation, and this permits a major simplification of the hovering design and performance problems.

The intercepts of the family of straight lines of Figure 5 on the axis of $C_T = 0$ are here called C_{Q_o}. The theoretically derived equation (18), based on optimum blade twist, uniform blade chord, and uniform drag coefficient, results in

$$C_{Q_o} = \frac{\sigma c_{de}}{8} \qquad \text{- (19)}$$

For tapered blades of various amounts of taper, twist, and thickness ratio, c_{de} may be interpreted as the "effective" uniform drag coefficient (the uniform drag coefficient on a uniform chord blade of optimum twist which would give the observed C_{Q_o}). Thus defined c_{de} becomes a function of taper and twist, as well as thickness ratio. Data on wing drag indicate that the usual small amounts of taper and twist have minor effects on wing drag, but thickness ratio is a major effect. The effect of wing thickness ratio on profile drag coefficient has been fairly thoroughly explored: for a given Reynolds and Mach number it consists of a skin friction drag term (partly laminar but usually mostly turbulent, depending on a large number of other factors), plus an additional term due to "eddy drag" resulting from low pressures in the rear portion of the airfoil. The minimum section drag coefficient (due to skin friction) at $R_e = 6 \times 10^6$ is seen in reference 1, page A2a:20 to be about 0.004 for smooth airfoils, 0.008 for rough airfoils; the incremental section drag due to thickness is roughly proportional to thickness ratio t/c, more accurately proportional to $(t/c)^{3/2}$. The increment is about fifty per cent over the turbulent skin friction for (t/c)= 21 per cent.

Equation (19) suggests that for helicopter rotor blades of a

given taper, twist, and thickness ratio, C_{Q_o} should be proportional to the "effective solidity" calculated from $\sigma = bc_e/\pi R$, with c_e as an "effective chord" defined as in the notation (page vii). (An alternate "effective chord" based on torque rather than thrust, as used in some of the earlier NACA reports, would be more rational here, but in practice the difference is small, and for the purposes of this study can be neglected.)

The relationship between C_{Q_o}, c_{de}, and σ suggested by equation (19) is investigated in Figure 6, where C_{Q_o} intercepts from Figure 5 are plotted against σ. The intercepts are not very accurately determinable if it is granted that lines of slightly different slopes in Figure 5 ($k_h = 1.21 \pm 0.05$) fit the test data nearly equally well. Accordingly boxes instead of points are plotted in Figure 6 showing the range of values of C_{Q_o} for each σ that a careful observer might read from the test data. Much more data than are now available would be desirable. Preferably the tests should be run on families of rotors of a given number of blades, keeping the blade twist optimum, and keeping the blade thickness ratio, surface condition, and planform constant while the solidity is varied. Only two points are shown in Figure 6 where this has been done; these are the points on the line labeled $10^5 C_{Q_o} = 150\sigma$, corresponding to two-blade rotors of twenty per cent thickness ratio. For two smooth surfaced fifteen per cent thick three-blade rotors, the points (boxes) lie on or somewhat below the line labeled $10^5 C_{Q_o} = 100\sigma$.

For purposes of preliminary design, it is desirable to provide a simple formulation of a readily achievable goal in the relationship

between C_{Qo} and σ, and also to recognize the extent to which actual construction may fall short of this goal. On the basis of Figure 6, such a formulation, put in the form of equation (18), is

$$C_{Qo} = \frac{\sigma c_{de}}{8} = 0.0010\sigma \text{ to } 0.0015\sigma \quad - - - - - - - - - - - - - - - \quad (20)$$

The corresponding range of values of c_{de} is 0.008 to 0.012 which is considered to be in good agreement with test data on drag of tapered wings, taking account of the fact that the usual range of values of Reynolds Number for the outer half of full scale helicopter blades is in the range from 2,000,000 to 4,000,000.

Equation (18) can also be expressed in horsepower per 1000 pounds of gross weight in the same manner as equation (9) was converted to equation (10), yielding

$$p_h = \frac{1000}{550} \frac{\rho_o \sigma c_{de}}{8w} V_t^3 + \frac{1000}{550} \frac{k_h \sqrt{w}}{\sqrt{2\rho_o}} \quad - - - - - - - - - - - - - - - \quad (21)$$

which becomes, for $c_{de} = 0.008$ as above ($10^5 C_{Qo} = 100\sigma$), $k_h = 1.21$ as previously discussed, and with $v = V_t/100$ by definition

$$p_h = 4.32 \frac{\sigma v^3}{w} + 31.9 \sqrt{w} \quad - \quad (22)$$

Equation (22) is difficult to represent graphically because p_h is a function of three variables. One simplification is to divide through by $\sqrt[3]{\sigma}$, giving

$$\frac{p_h}{\sqrt[3]{\sigma}} = \frac{4.23\, v^3}{w/\sigma^{2/3}} + 31.9 \sqrt{w/\sigma^{2/3}} \quad - - - - - - - - - - - - - - - - \quad (23)$$

A still simpler equation results if one can approximate the variation of C_Q with σ by an equation of the form $10^5 C_Q = 450\sigma^{3/2}$, and this

possibility has been explored in reference 1, resulting in design charts given there on pages 5:22 and A2e:14, but the approximation can be good only for a narrow range of solidities, is difficult to justify theoretically, and experimental confirmation is lacking.

A hovering power chart plotted on the basis of equation (23) is shown in Figure 7, using $p_h/\sqrt[3]{\sigma}$ as ordinate and $w/\sigma^{2/3}$ as abscissa. Additional ordinate scales of p_h and additional abscissa scales of rotor diameter for W = 1000 pounds and sea level conditions are also provided for several common values of solidity. Tip speed is the parameter used in plotting equation (23). Other parameters involving speed limitations in forward flight and landing limitations are developed and discussed later.

(c) Analysis and Use of Flight Test Data.

Current practice of some helicopter manufacturers in making performance calculations is to plot flight test data on figure of merit against C_T/σ (or $2C_T/\sigma$) as shown in Figure 8. The definition of figure of merit given below equation (10) is often modified, as in reference 3, to give an ideal value of unity. Thus

$$M' = F_m/\sqrt{2} = 0.707\ C_T^{3/2}/C_Q \quad - - - - - - - - - - - - - - - - - - \quad (24)$$

Hovering rotor theory, as expressed by equation (18), may also be written

$$\frac{1}{M'} = \frac{1}{B} + \frac{\sqrt{2}}{8}\frac{c_{de}}{\sqrt{\sigma}}\left(\frac{\sigma}{C_T}\right)^{3/2} \quad - \quad (25)$$

where 1/B may be replaced by k_h if factors other than tip loss are considered. For a given σ, equation (25) can be plotted as a straight

line of $(1/M')$ is plotted as ordinate and $(\sigma/2C_T)^{3/2}$ as abscissa, and the flight test data of Figure 8 has been thus replotted in Figure 9. With this type of plot the factor k_h can be read as the intercept on the $(1/M')$ axis. In Figure 9, k_h is seen to be 1.15 to 1.24 for the Bell and Seibel flight test data respectively. A line corresponding to the high drag tower test data in Figure 6 (corresponding to $c_{de} = 0.012$ and $k_h = 1.21$) is also shown in Figure 8 and is seen to be in good agreement with the Bell and Seibel flight test data.

To provide a rational basis for correcting flight test data to other than the test values of solidity and drag coefficient, it is the practice of reference 13 to let B = 1 in equation (25) and thus express it in the form

$$\frac{1}{M} - 1 = \frac{\sqrt{2}}{8} \frac{c_{de}}{\sqrt{\sigma}} \left(\frac{\sigma}{C_T}\right)^{3/2} \qquad (26)$$

and to use test results M'_1 plotted for a $c_{de} = c_{de_1}$ for some other rotor of estimated $c_{de} = c_{de_2}$, the calculated M'_2 based on equation (26) is

$$\frac{\frac{1}{M'_2} - 1}{\frac{1}{M'_1} - 1} = \frac{c_{de_2}}{c_{de_1}} \qquad (27)$$

and similarly the correction to other than the test values of solidity is given by

$$\frac{\frac{1}{M'_2} - 1}{\frac{1}{M'_1} - 1} = \frac{\sqrt{\sigma_1}}{\sqrt{\sigma_2}} \qquad (28)$$

The foregoing analysis constitutes a derivation of the solidity and roughness corrections as given in reference 13.

By this analysis it would appear that the correction method of reference 13 would be improved in accuracy if equation (25) rather than equation (26) were used, since the assumption of $k_h = 1$ is not justified by the data and an experimental value for k_h of about 1.2 would be better. This would correspond to replacing $(1/M' - 1)$ by $(1/M' - 1.2)$ in equations (27) and (28). Since the usual range of values of $1/M'$ is 1.5 to 1.8, the error due to using 1 instead of 1.2 is 25 to 40 per cent. If, however, equations (27) and (28) are used only for small corrections $\left(\frac{c_{de_2}}{c_{de_2}} \text{ and } \sqrt{\frac{\sigma_1}{\sigma_2}}\right.$ between 0.8 and 1.2) the error in the corrected values of M' for a given C_T/σ will usually be under six or seven per cent, and this error is usually within the accuracy of flight test measurements, so the correction procedure of reference 13 is judged of adequate accuracy.

An equation which fits well the Bell and Seibel flight test data thus differs from equation (22) only in the constant in the profile power term. With the higher profile torque measured in flight, equation (22) becomes

$$p_h = 6.48 \frac{\sigma v^3}{w} + 31.9 \sqrt{w} \quad - (29)$$

Equation (29) could be plotted in the form of a chart similar to Figure 7 where equation (22) was plotted, but an alternate form is developed in the next chapter for closer integration with speed limitations in forward flight.

For <u>tandem rotors</u> arrangements, such as Figure 1(b), reference 13 reports that p_h (hovering horsepower per 1000 pounds of gross weight) is generally one per cent to four per cent less than for a single rotor

machine like Figure 1(a). In forward flight, the tandem rotor requires more induced power for a given gross weight, and reference 13 estimates the increase in induced power over the single rotor configuration as between 35 per cent and 50 per cent. At normal cruising speeds, however, induced power is small, and body (parasite) drag may be smaller for a given payload, so that only a small net increase in power (estimated in reference 13 as three to nine per cent) is likely to be involved in changing from single rotor to tandem rotor configurations. For preliminary design calculations it is judged to be approximately correct to use single rotor hovering data and equations for tandem rotor configurations, and for forward flight to increase the induced power on the basis of the area of air stream affected by the rotors.

CHAPTER III

SPEED LIMITATIONS

Flight experience with cyclic pitch controlled helicopters has shown that approach of stall of the retreating blades as forward speed is increased provides one major limitation on high speed flight. A second major limitation is the "compressibility drag rise" of the advancing blades associated with local Mach numbers exceeding unity and with the formation of local shock waves, analogous to the "tip speed loss" of propellers, but occurring at much lower forward speeds because the tip velocity and forward velocity are much more nearly in the same direction than for an airplane propeller.

(a) Retreating Blade Stall Limitation

Current practice in calculating limitations due to retreating blade stall, for rectangular untwisted blades, is presented in reference 3, which gives two families of charts of μ against C_T/σ with $P/L = \left(\frac{D}{L}\right)_o + \left(\frac{D}{L}\right)_i + \left(\frac{D}{L}\right)_p + \left(\frac{D}{L}\right)_c$ as a parameter for 12° and 16° angle of attack respectively of the retreating blade at $\Psi = 270°$. Evidence is also presented that 12° retreating blade angle of attack is a permissible initial stall, and that 16° involves a prohibitive drag rise. The charts of reference 3 are replotted in Figure 10 using $\sqrt{C_T/\sigma}$ as an ordinate instead of C_T/σ. Only the lines for P/L = 0.2 and 0.4 are plotted, corresponding to level high speed flight of low and high powered helicopters respectively.

Note in Figure 10 that the lines for P/L = 0.3 are closely approximated by the empirical equations

$$\text{for } \alpha_{270^\circ} = 16^\circ,\ \sqrt{C_T/\sigma} = 0.475 - 0.63\mu_{LS} \quad \text{- - - - - - - - - - - (30)}$$

$$\text{for } \alpha_{270^\circ} = 12^\circ,\ \sqrt{C_T/\sigma} = 0.425 - 0.63\mu_{LS} \quad \text{- - - - - - - - - - - (31)}$$

Also plotted in Figure 10 is the "permissible" or "rotor limit" value of μ adopted in reference 13. The plot in reference 13 is inaccurate, however, because the "semi-empirical" equation there given corresponds to a straight line on Figure 10 about midway between equations (30) and (31). Reference 13 considers this to be a valid limit based on flight tests of Bell helicopters and repeatable independently within three per cent by several pilots. The Bell helicopter rotor limit of Figure 10 is considered in reference 13 to be semi-empirical rather than completely empirical because it can be derived on the basis of the rather crude assumptions 1) that each blade behaves like a rotating wing of finite aspect ratio based on the outer half of the blade, 2) that the retreating blade carries the same lift as the advancing blade, and 3) that the rotor limit is reached when the local $c_{l\ max} = 1.3$ at a station $r = 0.85R$ on the retreating blade. Chapter I of this dissertation points out the fact that assumption 2) does not correspond exactly to the physical facts. Reference 1 uses assumption 1) and concludes that the hovering torque and thrust coefficients are related by an equation of the form $C_Q(C_T^2)$, whereas a more nearly correct integrated blade element analysis gives the closer approximation $C_Q(C_T^{3/2})$. The reasonableness of the semi-empirical approximation is considered unimportant, however, because equations (30)

and (31) need merely be considered as specifying well established retreating blade stall limits for severe and incipient stall respectively.

Since reference 13 finds flight test rotor limits beyond "incipient" stall permissible, an upper limit beyond which designs must not go is obtained with equation (30) rather than (31). Equation (30) may be solved for the limiting speed of incipient stall V_{LS}, thus

$$V_{LS} = 0.75\Omega R - \frac{\Omega R}{0.63}\sqrt{\frac{C_T}{\sigma}}\sqrt{\frac{1}{\rho_o}}$$

or

$$V_{LS} = 0.75\Omega R - 32.5\sqrt{\frac{w}{\sigma}} \quad \text{- (32)}$$

Equation (30) was written for P/L = 0.3; to cover the range of values from P/L = 0.2 to 0.4, the slope need be varied only about plus or minus seven per cent and the corresponding range of equation (32) is

$$V_{LS} = (0.75 \pm 0.05)\Omega R - (32.5 \pm 2.5)\sqrt{w/\sigma} \quad \text{- - - - - - - - - - (33)}$$

Since engineers most often think of speed limitations in miles per hour (though sometimes knots), it is considered desirable to rewrite equation (33) in such units giving

$$mph_{LS} = 0.51\Omega R - 22\sqrt{w/\sigma} \pm 7\% \quad \text{- - - - - - - - - - - - - - - - - - (34)}$$

Equation (34) is plotted in Figure 11 so that lines of constant mph_{LS} can be read and transferred to the hovering design chart, Figure 7. Two lines are shown on Figure 3 for each value of mph_{LS} to cover the range of solidities from 0.04 to 0.09. Having the stall-limited speeds on the hovering power chart is of great help to the designer who must select

design parameters to meet a performance specification which includes level high speed.

In reference 13 it is noted that both p_h [equation (29)] and mph_{LS} [equation (34)] are functions of v, w, and σ and can therefore be solved simultaneously to eliminate one of the variables. This is considered desirable because the usual design problem involves a specified level high speed which must <u>not</u> be limited by stall of the retreating blades. Eliminating successively σ, w, and v in this manner gives the following three equations:

$$p_h = 6.48v^3 \left(\frac{22}{51v - mph_{LS}}\right)^2 + 31.9\sqrt{w} \quad \text{- - - - - - - - - - - - - (35)}$$

$$p_h = 6.48v^3 \left(\frac{22}{51v - mph_{LS}}\right)^2 + 31.9\sqrt{\sigma}\frac{51v - mph_{LS}}{22} \quad \text{- - - - - - - (36)}$$

$$p_h = \frac{6.48}{w/\sigma}\left(\frac{mph_{LS} + 22w/\sigma}{51}\right)^3 + 31.9\sqrt{w} \quad \text{- - - - - - - - - - - - - (37)}$$

Equation (35) is essentially the equation used in reference 13 as a basis for discussion of the effects of parameters on performance. For a given constant rotor limit speed mph_{LS}, equation (35) may be plotted as a network chart of p_h vs. v with w and σ as parameters. Such a chart is Figure 12 of this dissertation (for mph_{LS} = 100 mph) or Figure 12 of reference 13 (for rotor limit speed = 110 mph), which also includes a useful additional chart for constant payload.

In choosing coordinates for graphical representation of the hovering power requirements for a <u>given rotor limit speed</u>, it is considered highly desirable here (as also in reference 13) to use Bhp/W as the y-coordinate. The choice of the x-coordinate may be either v, w,

or σ, as implied by equations (35), (36), and (37) or possibly some combination of these such as w/σ. Figure 12 has used v, but either w or w/σ is considered preferable, and $\sqrt{w}$ may be best of all, because the resulting chart consists of a family of straight lines, and a single rotor diameter scale can conveniently be added. Such a plot is Figure 13. Note in Figure 13 that a wide range of constant rotor limit speeds (mph_{LS} = 50 to 200) can be added without confusion, though lines of constant solidity for each mph_{LS} were found confusing, so numerical values of solidity were spotted in.

Reference 13 considers that v and w may well be chosen as primary variables, and that σ "drops in the bucket," but inspection and use of Figure 13 shows that it is at least equally desirable to let v "drop in the bucket" as long as compressibility drag rise speeds are not exceeded.

(b) Advancing Blade Shock Limitation.

For a hovering rotor the tip speed limit due to compressibility drag rise would be the same as for an airplane propeller operating under static thrust conditions if it were not for the following important differences: 1) helicopter blades are usually made thicker (t/c greater) to minimize retreating blade stall and flutter problems, and 2) helicopter blades operate at a much lower lift coefficient for efficient designs. A quantitative comparison of limiting tip Mach numbers is presented in reference 8, where it is seen that at low lift coefficients, M_{tip} for propellers with very thin tips may run as high as 0.88, whereas M_{tip} for thin helicopter blades (nine per cent thick) can rarely exceed 0.83, and a typical range of values for (t/c_{tip} = 0.12 to 0.15) is

M_{tip} = 0.75 to 0.80.

For a helicopter in forward flight, the combined effects of rotative speed, forward speed, and cyclic angle of attack variation, as reported in reference 6, may be critical anywhere in the range of angles from $\psi = 0$ to $\psi = 180^{o}$, but calculations made at $\psi = 90^{o}$ (advancing) will usually suffice for preliminary design work. At $\psi = 90^{o}$, $M_{tip} = (V + \Omega R)/a$.

The preliminary designer should know whether a helicopter flying at the stall-limited speed mph_{LS} will or will not run into compressibility drag rise problems. For standard sea level conditions, where a = 1120 feet per second and M_t is limited to 0.75 to 0.80, the resultant velocity $V + \Omega R$ is limited to (0.75 to 0.80)1120 = 840 to 900) feet per second. Designating the limit due to <u>both</u> retreating blade stall and advancing blade shock by the triple subscript $(\ )_{LSc}$, it follows that

$$(\Omega R)_{LSc} = (840 \text{ to } 900) - 1.467\ mph_{LS} \quad - - - - - - - - - - - - \quad (38)$$

This limit is shown on the hovering design chart, Figure 7, as a supplement to the family of lines of constant mph_{LS}; the area beyond $M_{tip} = 0.80$ is crosshatched as a warning to the designer that the area must be avoided in selecting design parameters.

In the alternate hovering power chart, Figure 13, it was found convenient to take account of equation (38) by simply deleting from the chart any values of V_t which exceeded $(\Omega R)_{LSc}$ as given by equation (38).

CHAPTER IV

BLADE LIFT COEFFICIENTS FOR HOVERING POWER CHARTS

A useful addition to a hovering power chart would be a family of lines of constant mean blade lift coefficient $\overline{C}_{Lb}$. The mean blade lift coefficient is a useful concept for two reasons: 1) there is an optimum mean blade lift coefficient for minimum power for a given thrust of a given rotor, just as there is an optimum minimum power lift coefficient for a wing of finite aspect ratio, and 2) the mean blade lift coefficient cannot greatly exceed the static $C_{L\ max}$ in cushioning the possible shock of a power-off landing.

The "mean blade lift coefficient" is defined in reference 3 by the equation

$$W = \overline{C}_{Lb} \int_0^R b\tfrac{1}{2}\rho(\Omega r)^2 c\,dr \quad - \quad (39)$$

which for a uniform chord rotor integrates to

$$W = \overline{C}_{Lb}\Omega^2\ R^3 bc/6 \quad - \quad (40)$$

combined with the usual definition of thrust coefficient C_T, equation (40) becomes

$$\overline{C}_{Lb} = 6C_T/\sigma \quad - \quad (41)$$

It is desirable to include the blade lift coefficient in the hovering power equations (22) and (29), either of which may be written

$$p_h = k_1 \frac{v^3}{w/\sigma} + k_2\sqrt{w} \quad \text{-----------------------} \quad (42)$$

where $k_2 = 31.9$ and $k_1 = 4.32$ or 6.48 for low and high drag blades respectively. Using $C_T = 0.042\ w/v^2$ by definition and using equation (41), equation (42) may be written

$$p_h = 0.252 k_1 v/\overline{C}_{Lb} + k_2\sqrt{w} \quad \text{---------------------} \quad (43)$$

In the hovering power chart of Figure 13, each diagonal line corresponds to a specified v, so a value of $\overline{C}_{Lb}$ can be added to each line. For example, for $mph_{LS} = 100$ and $v = 5$ the first term of equation (43) is about 17, so this line on the chart can be also labeled $\overline{C}_{Lb} = (0.252 \times 6.48 \times 5)/17 = 0.48$.

In the hovering power chart of Figure 7, which is plotted from equation (23) using $w/\sigma^{2/3}$ as abscissa, lines of constant $\overline{C}_{Lb}$ can also be added. It may be seen, however, by dividing equation (43) by $\sqrt[3]{\sigma}$ that straight lines of constant $\overline{C}_{Lb}$ can be drawn only for $v/\sqrt[3]{\sigma}$ also constant. It is accordingly judged not particularly useful to add such lines to the chart, though it is useful to note that the region of high blade lift coefficients is the lower right hand region of the chart, and that this region should be avoided if a margin of lift is to be left for pulling up after an autorotative descent without power.

It is also useful to note that the ratio of hovering induced power to hovering profile power, here designated as r_h, may be calculated from the ratio in the two terms in equation (42) as

$$r_h = \frac{k_2}{k_1}\frac{w^{3/2}}{\sigma v^3} \quad \text{-------------------------} \quad (44)$$

From the definition of C_T, it may also be noted that

$$C_T^{3/2} = (0.042)^{3/2} \, w^{3/2}/v^3$$

Hence

$$r_h = \frac{k_2}{k_1 \sigma} \left(\frac{C_T}{0.042} \right)^{3/2} \qquad \text{- (45)}$$

which may also be written

$$r_h = \frac{k_1}{k_2 (0.252)^{3/2}} \sqrt{\sigma} \, \bar{C}_{Lb}^{3/2} \qquad \text{- - - - - - - - - - - - - - - - - - (46)}$$

For a helicopter operating at an approximately constant value of $1000C_T$, which is often the case, equation (45) may be used to calculate r_h. Lines of constant r_h can conveniently be added to Figure 13, though a complete family of such lines might prove more confusing than helpful; broken lines for $r_h = 1$ and $r_h = 2$ are shown in Figure 13. A more complete family of lines of constant r_h is desirable for a working chart, because r_h is one of the key parameters in the forward flight analysis presented later.

Lines of constant r_h obtained by substituting equation (44) in equation (42) are plotted in Figure 7. Equation (46) stated that such lines are also for constant values of $\sqrt[3]{\sigma} \, \bar{C}_{Lb}$. A line for $\bar{C}_{Lb} = 1.4$ for $\sigma = 0.09$ is shown on Figure 7 as a hovering stall limit; for $\sigma = 0.04$ the line is only about one-eighth inch on the chart to the left, so the line is labeled $\bar{C}_{Lb} \cong 1.4$ and is crosshatched to indicate a limit of practical design.

CHAPTER V

USE OF HOVERING POWER CHARTS

Two hovering power charts, Figures 7 and 13, have been developed in the preceding analysis.

Figure 7 is based on low-drag three-blade data, for which $10^5 C_{Qo} = 100\sigma$ in Figure 2, and is a plot of $p_h/\sqrt[3]{\sigma}$ versus $w/\sigma^{2/3}$.

Figure 13 is based on high-drag two-blade data, for which $10^5 C_{Qo} = 150\sigma$ in Figure 2, and is a plot of p_h versus $\sqrt{w}$.

Either type of plot could have been made with either group of test data; the combinations are arbitrary; many other combinations are possible.

The designer will normally select the expected blade drag range and the type of plot on the basis of experience. The use of Figure 13 for proposed new two-blade designs is conservative and convenient.

Note that both charts permit showing two regions of design to be avoided: 1) the region of very high horsepower per 1000 pounds of gross weight, where the power plant weight, even with turbines, will be high, and little lift will be available for payload, and 2) the region of very high disc loadings, where sinking speeds without power will be so high as to make shock-free power-off landings difficult or impossible.

Both charts also have rotor diameter scales for W = 1000 pounds and sea level conditions; scales for other gross weight and altitudes can easily be added by multiplying by the appropriate weight ratio or density ratio.

A feature of both charts is that they show quickly to the amateur or inexperienced designer what may have required long experience for professional designers to discover. For example, these charts show at a glance a number of design rules such as the following:

1) High level flight speeds are not possible without high tip speeds, closely approaching the compressibility drag limit.

2) High level flight speeds require large amounts of power, and the associated weight severely limits the payload.

3) Flight at the shock limit, even with the best of rotors, requires 65 to 100 horsepower per 1000 pounds of gross weight for the usual range of solidities of 0.04 to 0.09.

4) Hovering flight is seen in Figure 7 to be possible for a solidity of 0.04 with as little as 35 horsepower per 1000 pounds of gross weight, but helicopters so designed require very low blade loading and are severely limited in high speed by retreating blade stall. This type of helicopter also requires very large rotor diameter (35 feet to 40 feet for sea level hovering of a 1000 pound helicopter).

5) Small rotor diameter is achievable only with high tip speeds and high blade loadings, if the requirement of shock-free power-off landings is maintained; high engine power is also required.

6) The smallest achievable diameters are in the area to the right of Figure 7, involving also high solidity, (σ = 0.09) high power (p = 110 hp/1000 pounds), and high tip speed (around 700 feet per second). Such designs can carry very little payload, and are also hazardous to land because of high rate of descent.

7) A 175 mile per hour helicopter (and possibly a 200 mile per hour helicopter) can be built but it must have a large, heavy power plant and can carry very little payload. A 100 mile per hour helicopter can carry much more payload with a given power plant. Economical transport helicopters must be designed for relatively low values of level high speed.

Numerous other useful generalizations will become evident fairly quickly to the designer who makes frequent use of charts such as Figure 7 or Figure 13.

As an example of use of Figure 13, consider that it is desired to select a two-blade rotor of the Bell or Seibel type for a small helicopter of 1000 pounds gross weight with a rotor limit speed of 150 miles per hour at sea level, without exceeding thirty feet rotor diameter. The only tip speed lines plotted for this value of mph_{LS} are 600 and 700 feet per second. This is because 750 feet per second would be beyond the compressibility limit, with an advancing blade tip speed of 970 feet per second, whereas 400 feet per second would involve solidities in the range of 0.04 being off the chart to the right. Note in Figure 13 that minimum rotor power requires minimum disc loading, high tip speed, and minimum solidity. A satisfactory solution would be $V_t = 600$, $\sigma = 0.033$, and D = 28 feet, requiring seventy brake horsepower for the rotor to hover, but probably more than seventy horsepower to meet the high speed requirement (use Figure 20; note $p_a/p_h \simeq 1.4$ for a low drag helicopter, which would require an engine of at least

70 x 1.4 x 1.5 = 116 horsepower; with high body drag the engine power necessary approaches 200 horsepower, and with the usual weight ratios there might be no room for a pilot or payload in 1000 pounds of gross weight. For the level flight power requirement, a more accurate solution would involve preparing a new chart like Figure 20 based on the value of r_h read from Figure 13, which is about 1.4.

For one-man helicopters aiming at 500 pounds gross weight and 100 miles per hour with a diameter limit of fifteen feet, the equivalent 1000 pound diameter is $15\sqrt{2} = 21$ feet and a solution is seen in Figure 20 to be $V_t = 600$, $\sigma = 0.033$, $p_h = 70$ and $Bhp_r = 70/2 = 35$ horsepower, and even with a moderately high body drag Figure 20 shows that no additional power would be necessary to meet the high speed specification, and a motorcycle engine of about fifty horsepower might be satisfactory.

CHAPTER VI

HELICOPTER THEORY IN FORWARD FLIGHT

In forward flight at a small angle of climb or glide, the rotor disc is usually inclined at a small angle to the flight path. It is convenient to make the power calculations and analysis for level flight; surplus or deficiency of power then goes directly into climb or glide, as in airplane performance calculations.

A combination of momentum and blade element theories is commonly used in forward flight calculations. The profile drag of the rotor blades always increases with forward speed, as demonstrated in reference 2, Chapter VII, equation (23), by integrating around the azimuth angle, according to the equation

$$\frac{P'_p}{W} = \frac{\rho_o \sigma c_{de}}{8w} V_t^3(1 + \mu^2) = \frac{P_{hp}}{W}(1 + \mu^2) \quad - - - - - - - - - (47)$$

where P_{hp} is the hovering profile power per pound of gross weight, and μ is the advance ratio $V/\Omega R$.

A rotor tilt is necessary in level forward flight to provide a component of thrust to overcome the drag of helicopter body as well as to support the weight. The increased thrust necessary in forward flight can, however, be obtained with <u>less</u> power than is needed for hovering, because when the rotor is tilted <u>and</u> moving forward it entrains a much larger amount of air than when hovering. In fact, the usual expression written for the induced velocity at the disc in forward flight (v_{if}) is [reference 2, Chapter II, equation (24)],

$$v_{if} = \frac{W}{2\rho AV'} \qquad (48)$$

where V' is the vector sum of V and v_{if} (except for very low speeds $V' \simeq V$) and this same result could have been obtained by assuming that the air entrained is a horizontal stream of diameter equal to the rotor diameter, as in an airplane. Both references 2 and 4 quite properly point out that this is merely an assumption, that it cannot be proved, and that its use is justified on the grounds that it appears to be verified by flight tests, though separation of induced from profile effects in flight tests is not possible.

Reference 2 points out that the ideal induced power per pound of gross weight is

$$\frac{P'_{i\ id}}{W} = \frac{DV}{W} + v_{if} \qquad (49)$$

where v_{if} is given by equation (48), and needs a correction factor k to get actual induced power per pound, and D is not only the body drag but also the additional drag due to the rotor blades associated with the additional thrust necessary for forward flight, and is given by reference 2, Chapter VII, equation (27) for uniform chord blades as

$$D = \tfrac{1}{2}\rho V^2\left(f + \frac{c_{de}\sigma A}{2\mu}\right) \qquad (50)$$

Combining equations (48), (49), and (50) and including the correction factor k gives, for $V' \simeq V$ (except at very low speeds)

$$\frac{P'_i}{W} = \tfrac{1}{2}\frac{\rho V^3}{W}\left(f + \frac{c_{de}\sigma A}{2\mu}\right) + \frac{kW}{2\rho AV} \qquad (51)$$

In this study, as in reference 4, it is considered desirable to treat the first term of the right hand side of equation (51) as effectively part of the profile power, so that if

$$\frac{P}{W} = \frac{P'_p}{W} + \frac{P'_i}{W} \quad (52)$$

it can also be written

$$\frac{P}{W} = \frac{P_{pb}}{W} + \frac{P_i}{W} \quad (53)$$

where from equation (51)

$$\frac{P_i}{W} = \frac{kW}{2\rho AV} = \frac{k}{2\rho_o} \frac{w}{V_t} \frac{1}{\mu} \quad (54)$$

and from equations (47) and (51)

$$\frac{P_{pb}}{W} = \frac{\rho_o\, c_{de}}{8w/\sigma} V_t^3(1 + \mu^2) + \frac{\rho_o\, c_{de}}{4w/\sigma} V_t^3\, \mu^2 + \frac{\rho_o}{2w} \frac{f}{A} V_t^3\, \mu^3 \quad (55)$$

Defining $R_i = P_i/P_{hi}$ and $R_p = P_{pb}/P_{hp}$, equations (54) and (21) give

$$R_i = \frac{14.5}{\mu} \frac{k}{k_h} \frac{\sqrt{w}}{V_t} \quad (56)$$

and equations (55 and (21) give

$$R_p = 1 + 3\mu^2 + 4 \frac{f}{c_{de}\, A\sigma} \mu^3 \quad (57)$$

though reference 2 suggests 4.65 instead of 3 as the coefficient for μ^2 to allow for usual hub drag effects.

Equations (56) and (57) are general variations of induced and profile power with speed ratio, and are plotted in Figure 14. To get numerical values of the parameters in these equations, reference 2 assumed $k = k_h$, but this is considered doubtful, as k_h is a function of the blade tip loss factor B, which is judged to improve as the

helicopter moves forward. Writing also $v = V_t/100$, equation (56) becomes for $k_h/k = 1.16$

$$R_i = \frac{1}{8\mu} \frac{\sqrt{w}}{v}$$

or expressed in terms of C_T, with the conversion $1000C_T = 42w/v^2$

$$R_i = \frac{\sqrt{1000C_T}}{52} \frac{1}{\mu} \quad \text{- -} \quad (58)$$

Equation (58) is plotted for each of five numerical values of $1000C_T$ in the common flying range of 1.5 to 6.

In reference 1 the ratio $500f/A\sigma$ has been called f* and a range of $f/A\sigma$ from 0.1 to 0.3 was judged to cover the extremes of body drag of current helicopters. The numerical value 500 corresponds to $4/c_{de}$ in equation (57), and corresponds therefore to $c_{de} = 0.008$ which was found in equation (19) to be applicable to some of the test data studied here. The range of values of $\frac{f}{c_{de}\ A\sigma}$ corresponding to the above range of values of $f/A\sigma$ is from 12.5 to 37.5, and lines for these values as well as for 25 are plotted in Figure 14.

To get a general power required graph from Figure 14 it is necessary to assume a value (or a series of values) of the hovering power ratio $r_h = P_{hi}/P_{hp}$ since the general ratio of level flight power to hovering power is from previous definitions

$$R^* = \frac{R_p + r_h R_i}{1 + r_h} \quad \text{- -} \quad (59)$$

One obvious choice of r_h is the "optimum line" value of 2 and R* has been calculated from Figure 14 for $r_h = 2$ and plotted in Figure 15; the graph has been simplified by plotting only the low and high drag lines,

omitting the medium drag lines of f/c_{de} $A\sigma = 25$. Similar graphs for $r_h = 1$, 3, and 5 are plotted as Figures 16, 17, and 18. The values of r_h are close enough together to permit linear interpolation between charts without serious inaccuracy.

An experimental check is desirable at this point in the study to be sure that the calculation procedures are in line with flight realities.

CHAPTER VII

CHECK ON TEST DATA IN FORWARD FLIGHT

Only a partial experimental check on the foregoing theory is possible by flight tests. This is because the induced and profile power cannot be measured separately, and even though the total power is measured accurately (within a few per cent), its distribution between the induced and profile components, which determines the ratio $r_h = p_{hi}/p_{hp}$, is a major factor determining the shape of the graph of $R^* = p/p_h$ against advance ratio μ.

Another limitation on experimental checks is that very few test data are available in which the body drag has been measured as well as rotor power. In fact, only one such test is known to the author of this dissertation (reference 10); the results of this test are plotted in Figure 19, along with calculations made as outlined on the figure and further explained below.

For the tests reported in Figure 19, the measured parasite drag area is reported as 23 square feet, presumably of drag coefficient 1.28; the corresponding equivalent flat plate area of unity drag coefficient is $f = 18$, and for $A = 1139$ square feet and $\sigma = 0.042$, $f/A\sigma = 0.375$. The value of c_{de} obtained from the minimum profile torque coefficient was 0.008; hence $f/c_{de}A\sigma = 0.375/0.008 = 47$ plus rotor hub drag, which is estimated to increase $f/c_{de}A\sigma$ to 50 (higher than the highest drag assumed in plotting Figure 14, but this was a very old high-drag helicopter).

In Figure 19, the measured hovering horsepower per 1000 pounds of gross weight was $p_h = 54 \pm 1$ with v = 4.5 to 4.8, corresponding to $1000C_{Th} = 4.7$ to 5.3. The forward flight tests were not quite at the same mean C_T, as $1000C_T$ for the forward flight tests ran from 3.9 to 5.3, with a mean value of 4.6. The distribution of the measured p_h of 54 between p_{hi} and p_{hp} may be made by calculating either p_{hi} or p_{hp} from the theory and subtracting from 54 to get the other. In general, these two methods do not agree without some special interpretation of the theory. Calculating p_{hi} from equation (9) without blade loss factor gives, for the measured w of 2.58 pounds per square foot, $p_{hi} = 26.7\sqrt{2.58} = 42.8$, leaving $p_{hp} = 54 - 42.8 = 11.2$; using a tip loss factor B = 0.97 as in reference 3, figure 4-4 and equation (36) of reference 3 gives $p_{hi} = 42.8/0.97 = 44$ leaving $p_{hp} = 10$. The corresponding values of $r_h = p_{hi}/p_{hp}$ are 3.8 and 4.4, and a mean value of 4.0 has been used for calculations based on the above.

Calculating p_{hp} as in equation (21) with $c_{de} = 0.008$ gives $p_{hp} = 6.4$ to 7.6, and $r_h = 7.3$ to 7.5, but this assumption is judged here, as it was in reference 10, to be unreasonable. Reference 10 concluded on analysis of the tests and trying to make them agree with the theory, that c_{de} must have been about 0.014, which would give $p_{hp} = 11.2$ to 13.2, leaving $p_{hi} = 42.8$ to 40.8, and giving $r_h = 3.1$ to 3.9. Corresponding to this assumption, a mean value of $r_h = 3.5$ has also been used as an alternative calculation in Figure 19. The flight test values are seen in Figure 19 to lie within the range of theoretical plots between $r_h = 3.5$ and $r_h = 4.0$ corresponding to the

most reasonable of the above assumptions.

These tests also provide a single-point check on the hovering power chart of Figure 7: for $w/\sigma^{2/3} = 21.3$ and $\Omega R = 450$ to 480 as tested, Figure 7 reads, for σ interpolated to 0.042, a value of $p_h = 59$ to 60 compared to the flight test measured value of 54. Note, however, in Figure 6 that the design line $10^5 C_{Q_o} = 100\sigma$, on which Figure 7 is based, lies somewhat above the test points for a three-blade rotor of $\sigma = 0.042$, so that the ten per cent excess given by Figure 7 in this case is in line with other tests, and is not considered objectionable because it is conservative for design.

CHAPTER VIII

CHARTS FOR CLIMB AND LEVEL HIGH SPEED

Since Figures 15, 16, 17, and 18 constitute graphs of power required for level flight against speed ratio μ for various values of r_h, they can be used for calculation of level high speed and climb in the same manner as for airplanes by adding a graph of power available from the engine at the rotor. The power available can be considered as the brake horsepower of the engine minus the gear, tail rotor, and fan losses, and both engine RPM and gear losses are substantially independent of speed of forward flight. Accordingly, level high speeds can be picked off of Figures 15 to 18 for a given ratio of p_a/p_h and this has been done in Figure 20 for the same upper and lower limits of drag and thrust coefficient as used in the other figures for the special case of $r_h = 2$. Similar graphs can be prepared for other values of r_h. Note in Figure 20, as would be expected, that the body drag is the major factor determining the high speed for a given ratio of available power to hovering power; the operating thrust coefficient is a minor factor.

Also, in the same manner as for airplanes, for a given ratio of p_a/p_h the maximum excess horsepower available for climb may be picked off the graph of power required and power available, the corresponding rates of climb being calculated in terms of the hovering power per 1000 pounds of gross weight. For any given value of p_h, such as the samples shown in Figure 21, the actual rate of climb in feet per

minute can be shown on a scale. Note in Figure 21 that neither body drag nor operating thrust coefficient is a major factor in determining the rate of climb. The values of μ corresponding to the best rate of climb values shown in Figure 21 for $r_h = 2$ can be picked off the general power required chart Figure 15 on which it was based. Figure 21 also shows the approximate maximum vertical rate of climb calculated on the simple assumption that any excess horsepower above that needed for hovering can be used for vertical climb. It is evident from Figure 21, and corresponds to the flight test fact, that much higher rates of climb are possible at small forward speeds than are possible vertically.

Figure 21 was based on $r_h = 2$ from Figure 15. Similar graphs for $r_h = 1$, 3 and 5 can be prepared from Figures 16, 17, and 18 if desired.

Figure 21 can also be reasonably accurately extrapolated to show the minimum power for zero rate of climb and also the negative rate of climb (rate of descent) with zero power available, but the usual minimum rate of descent calculated by this method involves a fairly steep flight path and a large angle between the plane of the rotor disc and the flight path so that the assumptions involved in the derivation of the theoretical equations are not very closely fulfilled, and rates of descent calculated by this method are open to some question. A special study of rates of descent and the conditions necessary to reduce the rate of descent to zero by collective pitch control is made in the next chapter.

CHAPTER IX

SINKING SPEED WITHOUT POWER

(a) Vertical Autorotative Descent.

None of the references consulted in connection with this problem claims an adequate theoretical treatment of the problem of vertical autorotative descent, though several (notably 2, 3, and 4) present good physical pictures of what is happening to the air under such conditions and of the reasons why neither the simple momentum theory nor the blade element theory, nor any combination of them, can be readily applied so as to correspond to the observed facts.

The momentum theory, which considers a stream of air of definite boundaries passing through the rotor disc, is reasonably closely applicable to climb, to hovering, and to high rates of descent when the rotor is acting like a windmill, but at low rates of descent the air streamlines do not form a simple pattern, and this condition is usually described as the turbulent brake state of operation, or sometimes the "vortex ring state".

For high rates of descent, the assumption that the air passing through the rotor disc is brought to rest is shown in reference 2 to result in a limiting vertical descent velocity of

$$V_v = \sqrt{2/\rho_o}\sqrt{w} = 29\sqrt{w} \quad - - - - - - - - - - - - - - - - - \quad (60)$$

and experiments in reference 11 check this relationship within a few per cent [a constant of 28 instead of 29 in equation (60)] when the descent

was started from zero thrust at autorotative speed.

The difficulty in calculating the speed of rotor rotation in vertical autorotative descent is also well presented in reference 2, which points out the fact that under these conditions the inner third (approximately) of the blade is stalled, the middle third is exerting a net forward force (at high angle of attack) and the outer third (approximately) is exerting a net rearward force, to give zero net moment (if rotor is "free wheeling") about the rotor axis when the speed of rotation is stable. For this condition, a blade element analysis is numerically feasible, but no simplified analysis, like the "finite wing approximation" for hovering, has been presented. The results could be presented in a form similar to Figure 7, but this has not been done because vertical descents are seldom attempted even in emergencies, as much lower rates of descent are possible at a small forward speed for the same reason that much higher rates of climb are possible at small forward speeds as discussed in the preceding chapter.

(b) Descent in Autorotative Forward Flight.

It is suggested in reference 2 that the approximate rate of descent in autorotative forward flight be calculated by assuming that the level flight power equations (54) and (55) are applicable and that the power is supplied by gravity. This procedure is not considered fundamentally correct for at least two reasons: 1) the forces which determine the windmilling speed of a gliding rotor, as described above, are not considered, so the rotative speed of the rotor in power-off descent is not known, and 2) the angle between the plane of

the rotor disc and the wind velocity vector is not small, as assumed in forward flight theory.

On the other hand, if the descent starts with the rotor rotating at the design speed, either in hovering or forward flight, and if the pilot quickly sets the collective pitch in the best position for maintaining this rotative speed after the power is cut off, the rate of change of rotative speed may be very slow, particularly if the rotor inertia is large. Moreover, optimum cyclic pitch in the power-off glide may result in nearly the same power-speed relationships as in level flight, and if the approximation is not very good, a correction factor may reasonably be applied, for all the major variables are in the analysis in their proper places. Obviously this is an important and possibly very fruitful field for further research. For the purposes of this dissertation, the suggestion of reference 2 will be followed, as the primary purposes of this study (to indicate the design areas in which shock-free landing may be difficult) are well served by a fair approximation with empirical correction factors.

Accordingly, the minimum descent rates for both vertical and forward flight autorotative descents have been calculated and are plotted in Figure 22. The vertical descent rate is plotted from equation (60). The minimum autorotative descent rate in forward flight glides was calculated as follows on the basis of the argument developed in the paragraph above. For each of two values of r_h ($r_h = 2$ and $r_h = 3$) in a relationship can be determined between p_h and w from the hovering design charts. With $r_h = 2$ and 3 respectively, the values of p_h are

$$p_h = 47.8\sqrt{w} \quad \text{and} \quad p_h = 42.4\sqrt{w} \qquad \text{- - - - - - - - - - - - - - - - (61)}$$

The minimum powers necessary for level flight may be determined by multiplying equation (61) by R^*_{min} as read from Figure 15 and 17 (or calculated from the corresponding equations), and the minimum rate of descent on the basis of the assumptions explained above is, for sinking speeds in feet per second

$$V_{s\ min} = \frac{550}{1000} p_h\ R^*_{min} \quad - (62)$$

Selecting values of R^*_{min} from Figures 15 and 17 corresponding to the lowest and highest values of body drag ratio ($f/c_{de}A\sigma$) and operating thrust coefficient ($1000C_T$) gives four equations like equation (62) for each of equations (61), and these eight lines are plotted in Figure 22. For $r_h = 2$, values read from Figure 15 and the corresponding values of p_h/w and $\mu_{R^*_{min}}$ are given in the following table:

	High Drag $1000C_T = 6$	High Drag $1000C_T = 1.5$	Low Drag $1000C_T = 6$	Low Drag $1000C_T = 1.5$
R^*_{min}	0.70	0.55	0.625	0.505
$\mu_{R^*_{min}}$	.115	.10	.15	.13
$\frac{550}{1000} R^*_{min}\ p_h/\sqrt{w}$	18.4	14.5	16.5	13.3

The quantities in the last line above are the intercepts at $w = 1$ of four of the lines plotted on Figure 22. Similar calculations for $r_h = 3$ are seen in Figure 22 to give considerably lower rates of descent.

The rotor tip speeds implied by these calculations are shown in the top half of Figure 22 on the basis of equation (22) but as previously noted there is considerable doubt as to whether these speeds will actually be attained in flight since they are calculated for design level

flight conditions and are not based on a proper aerodynamic analysis of the windmilling action of the blades in autorotative forward flight.

Experimental check on the above analysis is available from published glide performance of a Bell H-13-B helicopter as discussed in reference 1. Both experimental and calculated points are plotted for comparison. Note at the top of Figure 22 that the gliding rotor windmilled at about fifteen per cent less tip speed than the design level flight condition read from Figure 7. This discrepancy is considered reasonable in view of the discussion in the preceding paragraph. Note also that in spite of the discrepancy in windmilling tip speed, both the actual vertical descent rate and the actual gliding descent rate are within ten per cent of the calculated values. It is judged that a statistical study of a large number of autorotative glide tests would show a considerably larger average discrepancy. It is claimed in reference 12 that autorotative glide tests are in good agreement with theory, but the theoretical calculations there presented do not attempt prediction of the autorotative tip speed, but rather use the tip speed as measured in the tests to predict the drag/lift ratio of the rotor, so they do not solve the designer's problem.

CHAPTER X

LANDING WITHOUT POWER

The principal safety feature of a helicopter which cannot be matched by any other heavier-than-air vehicle is its ability to land without power on rough ground completely without landing shock. Preservation of this feature in proposed new designs is currently (1954) one of the requirements of the Civil Aeronautics Administration for commercial licensing of helicopters, and military helicopter pilots are currently being instructed with a view to developing proficiency in this maneuver. The technique consists in first maintaining an autorotative glide at or near the minimum descent rate until within a short distance of the ground and then pulling up on the collective pitch control to reduce the vertical speed to zero (or in small areas of rough terrain to reduce the speed along the flight path to zero). This is known as the "flare" or "flare-up" maneuver.

Physically the flare-up maneuver involves using the rotary kinetic energy of the rotor to reduce the translational kinetic energy of the helicopter. The glide must be made at a mean blade lift coefficient considerably below $\bar{C}_{Lb\ max}$ for this to be possible, since the net deceleration, written as a negative acceleration, is from Newton's second law

$$-\frac{a}{g} = \frac{\bar{C}_{Lb\ max}}{\bar{C}'_{Lb}} - 1 \qquad (63)$$

where a is the vertical acceleration and $\bar{C}'_{Lb}$ is the mean blade lift

coefficient in the autorotative glide. Evidently from equation (63) when $\bar{C}_{Lb} = \bar{C}_{Lb\ max}$, no deceleration is possible. Equation (63) gives only the initial deceleration of a transient maneuver, because the increase in blade lift coefficient from $\bar{C}_{Lb}$ to $\bar{C}_{Lb\ max}$ also involves a large increase in blade drag coefficient which slows down the rotative speed of the rotor, and after a short time the rotor speed has dropped to the point where the pilot can no longer hold it off the ground with the collective pitch control. The helicopter must be landed by collective pitch control within this short time to avoid landing shock. The time which must be allowed the pilot for this maneuver is a statistical matter of pilot skill and training; a time of two seconds has been found acceptable. A small percentage of the pilots will fail to make shock-free landings with any arbitrary time allowance, but with reasonable shock absorbing capacity in the landing gear a negligible number of pilots will suffer bodily injury due to unskillful landings.

Predetermination by the designer of the design parameters necessary for shock-free landings is mathematically difficult because it involves parts of the blades operating beyond the stall where air forces are almost impossible to predetermine. Also the autorotative glide problem must be solved before the flare-up maneuver can be solved, since it is the starting point of the flare-up maneuver. An approximate analysis or even a qualitative analysis is still of value, because the hovering time without power is arbitrary, and determination of the conditions necessary for two seconds hovering plus or minus fifty per cent can still give a very useful result for preliminary design work and is particularly recommended for further study.

Calculations must start with the sinking speed determined in the preceding chapter. Note in Figure 22 that gliding at higher values of r_h (and hence at higher values of $\overline{C}_{Lb}$) permits lower rates of descent, but also provides less margin of lift coefficient ($\overline{C}_{Lb\ max} - \overline{C}_{Lb}$) for stopping. High values of sinking speed are seen in Figure 22 to be associated with high disc loadings. With high sinking speeds, the pilot must start the deceleration (by collective pitch control) at a large distance above the ground and this task is more difficult for the pilot the higher the sinking speed. With 32 feet per second sinking speed, for example, and with $\overline{C}_{Lb\ max}/\overline{C}'_{Lb} = 2$ available to produce 1g deceleration, the vertical sinking speed can be reduced to zero in one second and with constant deceleration this requires a vertical distance of sixteen feet. It is considered desirable to set some arbitrary limit of height beyond which the designer will not require the pilot to initiate the deceleration; sixteen feet is one possible such limit, though a much smaller value would be much safer. A limit of thirty feet per second rate of descent for an average drag helicopter operating at a thrust coefficient in the region of $1000C_T = 3$ to 4 is seen in Figure 22 to require a disc loading of under six or seven pounds per square foot with $r_h = 2$ to 3, corresponding to $\overline{C}'_{Lb}/\overline{C}_{Lb\ max} = 0.3$ to 0.5. With solidities in the region from 0.03 to 0.06, the corresponding blade loadings run over 100 pounds per square foot and this region has been designated on the design chart (Figure 7) by crosshatching as being questionable on account of high rates of descent.

High rotor inertia for a given helicopter gross weight, or more

particularly a high value of the factor

$$\text{Rotor momentum factor} = \frac{W_r}{W} \frac{k_r}{R} (\Omega R)_o \quad - - - - - - - - - - - (64)$$

is evidently desirable to keep the rotor from slowing down too fast after the collective pitch has been set up to $\bar{C}_{Lb\ max}$, but no attempt is made here to determine permissible limits of this factor in relation to other design parameters for the suggested limit of two seconds power-off hovering before the helicopter must be landed, as this is a major study suitable for an additional dissertation.

CHAPTER XI

WEIGHT ANALYSIS OF HELICOPTERS

The usual object in designing a helicopter is to create a vehicle which will carry persons or objects quickly and safely from one place to another. (The additional expense of a helicopter over an automobile or airplane is usually justifiable in the mind of the purchaser only if the places are inaccessible by automobile or airplane on account of lack of roads or landing fields, or if the travel by automobile is very slow because of heavy traffic.)

The persons or objects carried are known as "pay load"; fuel and oil (and usually pilot) are not included in the term pay load. In single seat helicopters, however, where the object is to transport the one person who pilots the helicopter (and also a small amount of baggage), the pilot is most of the "pay load". These relationships are expressed by the equation

$$W = W_{emp} + W_f + W_{pl} \quad - (65)$$

where W_{pl} is the pay load, W_f is the weight of fuel and oil, and W_{emp} is the "weight empty" of the helicopter. One way of measuring the overall achievement of a designer on his project is to calculate weight ratios such as W/W_{emp}, W/W_{pl}, or W_{pl}/W_{emp}, or their reciprocals, and some such ratios are listed for nine current helicopters in reference 1, Table 5:2. Another weight grouping sometimes used is to call $(W_f + W_{pl})$ the "useful load" (W_u) though certain items of weight, such as more or less

fixed equipment (radio, etc.) are classified by the designer as either part of the pay load or part of the weight empty, depending on what the designer wishes to prove.

Weight empty is commonly analysed into groups. Major groups are commonly rotor group, tail group, body group, landing gear group, power plant or propulsion system group, flight controls group, flight instruments group, electrical system group (sometimes included in power plant group), communications group, furnishings group, and sometimes others. The assignment of a particular weight item to a particular group must often be arbitrary, as no general definition applicable to all conceivable designs can say where one component ends and another begins. The dividing line between gear transmissions and rotor hubs, for example, is particularly difficult to generalize.

The problem of estimating helicopter component weights is further complicated by the fact that, in general, item weights are related to durability and fatigue, because much higher working stresses are satisfactory if a very short life is acceptable. If helicopters are designed like automobiles, for 50,000 miles to 100,000 miles (about 1000 hours for helicopters) between major overhauls, considerably heavier components are necessary than if 100 hours between overhauls is satisfactory. The military services, as reported in reference 7, are aiming for 1000 hours between overhauls, though they report at present (1954) various durabilities for various components, usually over 100 hours and always under 1000 hours. One military criterion for the usefulness of a helicopter is "availability" expressible numerically as the fraction

the time the helicopter can be flown, the remainder of the time being that necessary for repairs and maintenance. Military helicopter availability has been found very low compared with other military vehicles, including military airplanes. In general, high availability requires heavy component weights and cuts the pay load which can be carried with a given power plant.

In view of the above argument, it is evident that any attempt to forecast the weight of a particular helicopter component, or group of components, is necessarily subject to considerable error or scatter, even when the component weights are plotted against the variables which truly determine the weight.

The most essential features of a helicopter are a power plant and a rotor; for seven helicopters for which partial weight analyses are given in reference 1, Table 5:2, the rotor and power plant together constitute about sixty per cent ($\pm$ ten per cent) of the empty weight. The rotor usually consists of blades and hub, of which only the blade weight is believed amenable to rational or semi-rational analysis and such analysis is presented below. The principal component weights of the power plant group are usually engine and gear transmission. The engine weight is usually accurately known and supplied by the engine manufacturer. The gear transmission weight is also amenable to rational analysis and such analysis is also presented below. Other approximations for estimating weight empty at various stages of the preliminary design problem are also suggested in the next chapter.

(a) Rotor Blade Weight Estimates.

Lightness in a rotor blade is not an unmixed blessing for at least two reasons. Light rotors permit a low empty weight and hence larger pay load for a given power plant, but 1) durable rotors, which must be heavy, are a major contribution to "availability", and 2) heavy rotors are an aid to the flare-up maneuver in power-off landings. Also a little additional weight in the right places may be a major factor in reducing the likelihood of rotor blade flutter. On the other hand, large rotor diameter, if it can be achieved without excessive weight, is a major aerodynamic asset, and in general optimum aerodynamic design requires as large a rotor as is structurally feasible and permitted by storage space limitations, so that a rotor diameter limit is considered a basic part of any design specification.

Since a rotor blade is essentially a rotating wing, wing design experience and wing weight formulas may well be used as a guide to formulation of fules for estimating rotor blade weights. On the other hand, there are major differences in forces and supports between a helicopter blade and a cantilever airplane wing: centrifugal forces are a major factor for helicopter blades, and helicopter blades are usually mounted so as to either flap or teeter, and the resulting bending moments near the hub are greatly reduced compared with a cantilever wing or even with an airplane propeller blade. The lack of high bending moments near the hub and the presence of high centrifugal forces are, however, two compensating differences from a cantilever wing so consideration of cantilever wing weights is worth while.

Several studies of cantilever wing weights are reported in reference 1, appendix A5. The study by Joseph Kelley, Jr., summarized on page A5:3 of reference 1, may be approximated by the equation

$$W_w = 0.006 \left(\frac{Wn' \, sS}{t_R} \right)^{0.6} \quad - \quad (66)$$

where W_w is the wing weight in pounds, n' is the design load factor, t_R is the root thickness in feet, s is the wing span in feet, and S is the wing surface area in square feet. Applied to the blades of a helicopter, and neglecting variations in root thickness and design load factor, which are minor, and approximating the 0.6 power by the best fitting 0.5 power line, equation (66) becomes

$$W_b = k_b \, D^{3/2} \sqrt{W\sigma} \quad - \quad (67)$$

where k_b is an empirical coefficient to be determined. A chart with the coordinates indicated by equation (67) is plotted in Figure 23, and lines have been drawn for heavy and light rotors for best fit with the data in Table 5:2 of reference 1. Since the scatter of plotted points is no greater than the scatter found for equation (66) for wing heights, a more refined analysis is judged inappropriate until or unless a considerably greater amount of helicopter blade weight data becomes available.

(b) Gear Transmission Weights.

Studies of gear set weights in reference 7, reported by Mr. Stanley W. Baker of the Bergen Engineering and Development

Corporation, are presented graphically in the reference and the graphical results are representable by the following empirical equations

$$\text{For bevel gears} \qquad W_{gb} = (22 \text{ to } 36)(Q/10^4)^{0.7} \quad - - - - (68)$$

$$\text{For planetary gears} \qquad W_{gp} = (6.6 \text{ to } 12.5)(Q/10^4)^{0.7} \quad - - - (69)$$

where Q is the output torque in inch-pounds, W_{gp} is the weight in pounds of a planetary gear set, and W_{gb} is the weight in pounds of a bevel gear set. Mr. Baker points out that output torque rather than power is the proper basis for comparison, and that variation to less than the first power is at least partly caused by the necessity of using overweight standard parts in the small sizes. He also quite properly points out the fact that a planetary gear set can usually be built for about one-third of the weight of a bevel gear set; this fact greatly favors an engine with vertical shaft.

Collections of data for estimating weights of other components are usually maintained by manufacturers of helicopters, so that the weight of new models which represent only minor departures from existing models can be fairly accurately estimated. For entirely new designs, weight estimates must be much more approximate, and the design can only be developed by a converging series of approximate estimates based on general weight ratios such as are given in reference 1, Table 5:2. A suggested procedure, with illustrative example, is given in reference 1, and additional suggestions are presented in the following chapter.

CHAPTER XII

DESIGN TO A PERFORMANCE SPECIFICATION

Using the foregoing weight information and the charts provided in this dissertation, a helicopter designer can determine quickly a variety of rotor designs which will satisfy given payload and performance specifications. A recommended procedure is detailed and illustrated in reference 1. The philosophy of the procedure, and some useful variations of the procedure, are discussed below.

Step 1. For a specified payload, gross weight is some multiple of the payload, usually four to six times the payload, depending partly on the range or endurance. For a first approximate gross weight, five times the payload is suggested; better approximations will come later, and experience shows that the process will usually be converging.

Step 2. With a first approximate gross weight known, a power plant can be selected to satisfy the hovering condition at the specified hovering altitude using the hovering design chart (Figure 7 or a similar chart). Design at this point should be on the line of specified level high speed without retreating blade stall. Various combinations of diameter and solidity will satisfy the hovering requirement. If the diameter is limited by the specification, as it usually is by implication if not by specific statement, the upper limit of diameter may well be chosen; the solidity and horsepower will then be specified by the chart (Figure 7 or 13).

Step 3. With the diameter and the necessary horsepower known, a second weight estimate can be made, for a particular power plant, using average ratios of weight empty to power plant weight and adding fuel, oil, and pay load, and the diameter, solidity and power selection repeated as in Step 2.

Step 4. With a possible revised selection of power plant in Step 3, a third weight estimate can be made in more detail, taking account of gear transmission weight, rotor weight, and weights of other components in typical detailed weight analyses such as those presented in reference 1. For the third estimated weight smaller rotor diameters may also be considered, saving rotor weight but adding to power plant weight, using hovering performance (Figure 7) as a basis for selection.

Step 5. For the optimum hovering power plant and rotor, a check may well be made at this point to see whether there is sufficient power to meet the level high speed requirement, the climb requirement, and the climbing ceiling requirement, if any. If additional power is required, a fourth weight estimate may be necessary. In some cases, it will be found that the specified pay load and performance requirements cannot be met by any combination of design variables, and the specification must be changed or the solution abandoned. This is a very common result for an amateur designer who has set an over ambitious specification. More power requires more weight and more weight requires more power, and the pay load, which was the main objective, tends to disappear.

Step 6. Start detail design and structural analysis, and keep a continuous tally on the weight as the design details progress.

Following the foregoing processes for a number of designs will make the designer realize that low power plant weight is very important, whereas low specific fuel consumption is less important except for very long range helicopters. There is accordingly a growing demand for light, powerful engines for helicopters, with fuel economy a minor consideration. This leads first to the two-stroke cycle internal combustion engine, then to the gas turbine, and sometimes to the rotor tip burner, rotor tip pulse jet, or rotor tip ram jet, but all these are at present (1954) precluded by including in the specification some large average number of hours between major power plant overhauls (such as 500 or 1000 hours).

CHAPTER XIII

CONCLUDING REMARKS

Charts have been developed, consistent with current accepted theory, which permit a systematic preliminary design procedure that will satisfy specified forward flight as well as hovering performance with a given pay load.

The principal area in which improvements are needed in the procedure here outlined is in the field of more complete and more accurate analysis of the power-off glide, as shock-free landing from a power-off glide is considered to be the most outstanding safety and utility feature of a helicopter, and the field has thus far been only inaccurately explored.

REFERENCES

1. Wood, K. D. Airplane Design. Tenth Edition. Boulder, Colorado, University Bookstore, 1954. 397 pp.

2. Stepniewski, W. Z. Introduction to Helicopter Aerodynamics. Vol. 1. Performance. Morton, Pennsylvania, Rotorcraft Publishing Committee, 1950. 158 pp.

3. Gessow, Alfred and Garry C. Myers, Jr. Aerodynamics of the Helicopter. New York, Macmillan, 1952. 343 pp.

4. Dommasch, Daniel O. Elements of Propeller and Helicopter Aerodynamics. New York, Pitman Publishing Corporation, 1953. 178 pp.

5. Harris, R. J., L. H. Sloan and K. W. Ulrich. Typical Helicopter Performance Calculation. Morton, Pennsylvania, Rotorcraft Publishing Committee, 1952. 43 pp.

6. National Advisory Committee for Aeronautics, Conference on Helicopters, May 12, 13, 1954. A Compilation of the Papers Presented, (some security classified).

7. Morris, I. Sewell (Editor), Commanding Officer, Transportation Corps, Army Aviation Field Service Office, 420 Locust Street, St. Louis 2, Missouri. Summary of Presentations, Conference and Symposium, Hotel Statler, St. Louis, Missouri, May 10 to 12, 1954.

8. Stuart, Joseph III. Helicopter Rotor Performance Possibilities. Proceedings of the Seventh Annual Forum, American Helicopter Society, 2 East 64th Street, New York 21, New York. 159 pp.

9. Wood, K. D. Technical Aerodynamics. Second Edition. New York, McGraw-Hill Book Company, Inc., 1947. 472 pp.

10. Gustafson, F. B. and Alfred Gessow. Analysis of Flight Performance Measurements on a Twisted Plywood-Covered Helicopter Rotor in Various Flight Conditions. Technical Note No. 1595, National Advisory Committee for Aeronautics. June 1948. 42 pp.

11. Slaymaker, S. E., Robert R. Lynn and Robin B. Gray. Experimental Investigation of Transition of a Model Helicopter Rotor from Hovering to Vertical Autorotation. Technical Note No. 2648, National Advisory Committee for Aeronautics, March 1952. 29 pp.

12. Gessow, Alfred and Garry C. Myers. Flight Tests of a Helicopter Autorotation, Including a Comparison with Theory. Technical Note No. 1267, National Advisory Committee for Aeronautics, April 1947. 24 pp.

13. Brown, Eugene. Helicopter Performance and Aerodynamics. Bell Aircraft Corporation, Helicopter Division Document, 1954.

14. Seibel, Charles M. Aerodynamics Report for Single Place Helicopter. Seibel Helicopter Company. 26 February 1951.

15. Nikolsky, Alexander A. Notes on Helicopter Design Theory. Princeton University Press, 1944.

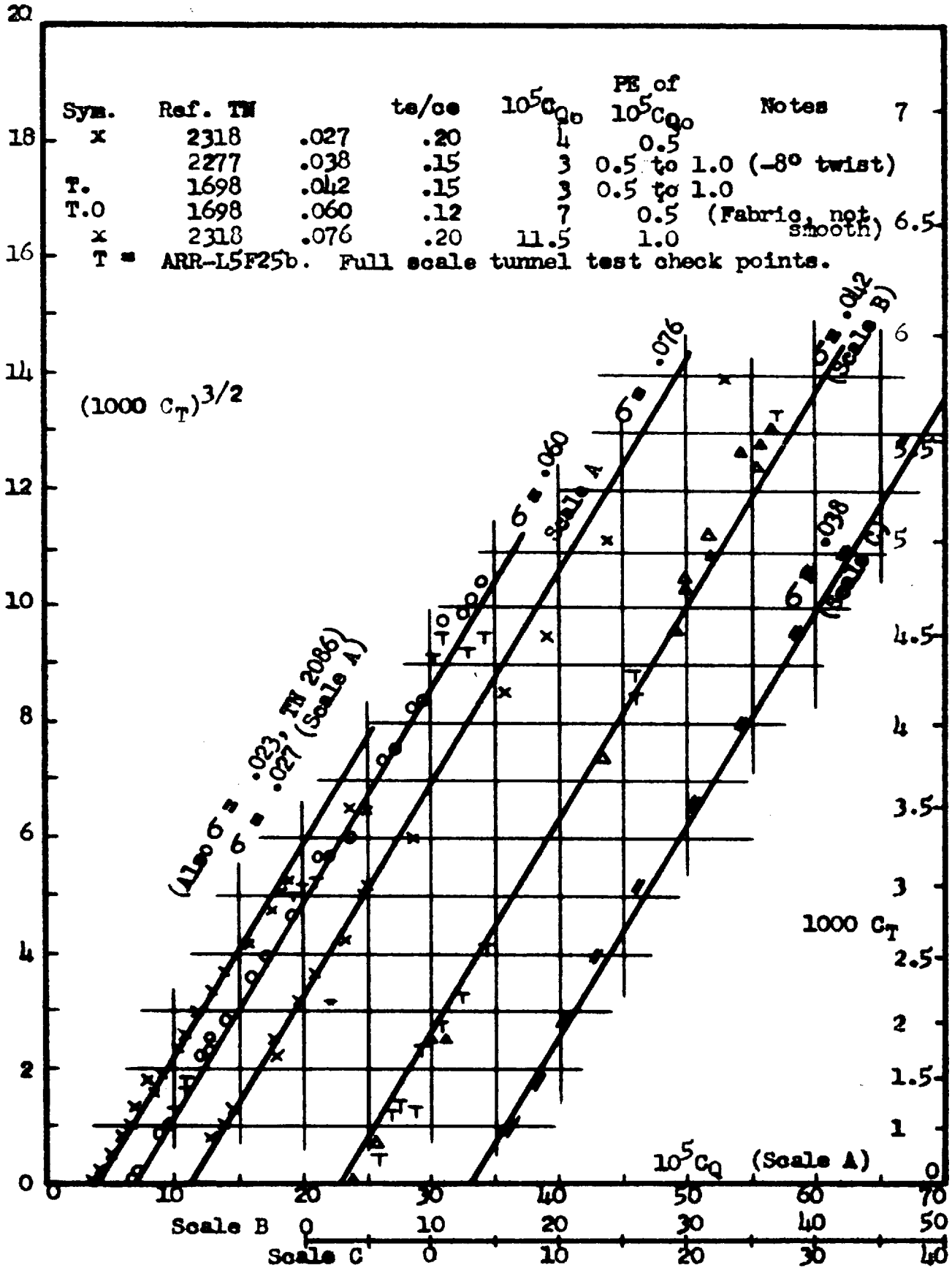


Figure 5. Helicopter Tower Test Data Fitted by Family of Straight Lines of Form $10^5\ C_Q = 10^5 C_{Qo} + k\ (1000 C_T)^{3/2}$, with $k = 2.7$

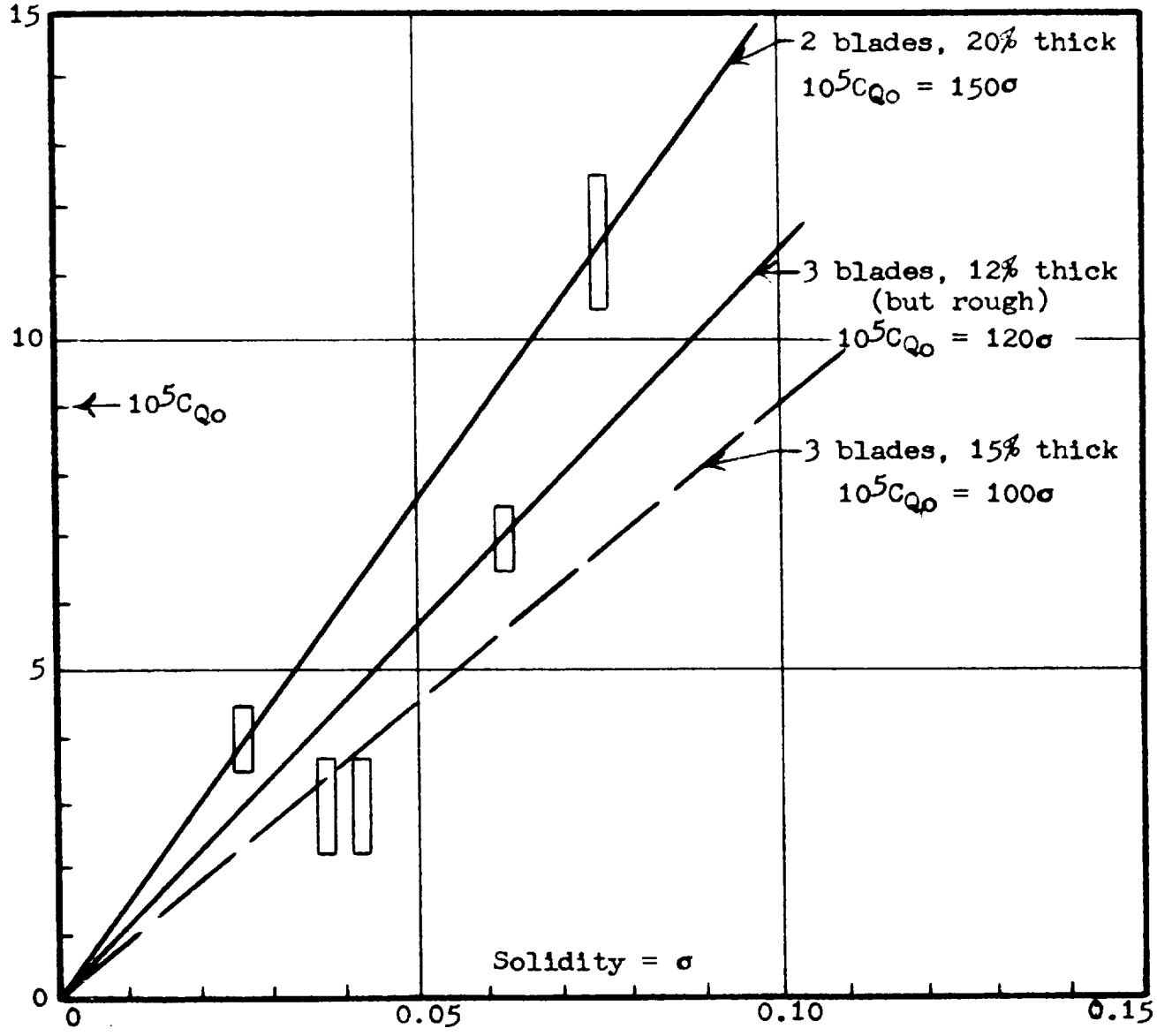


Figure 6. Intercepts C_{Qo} from Figure 5 Plotted Against σ

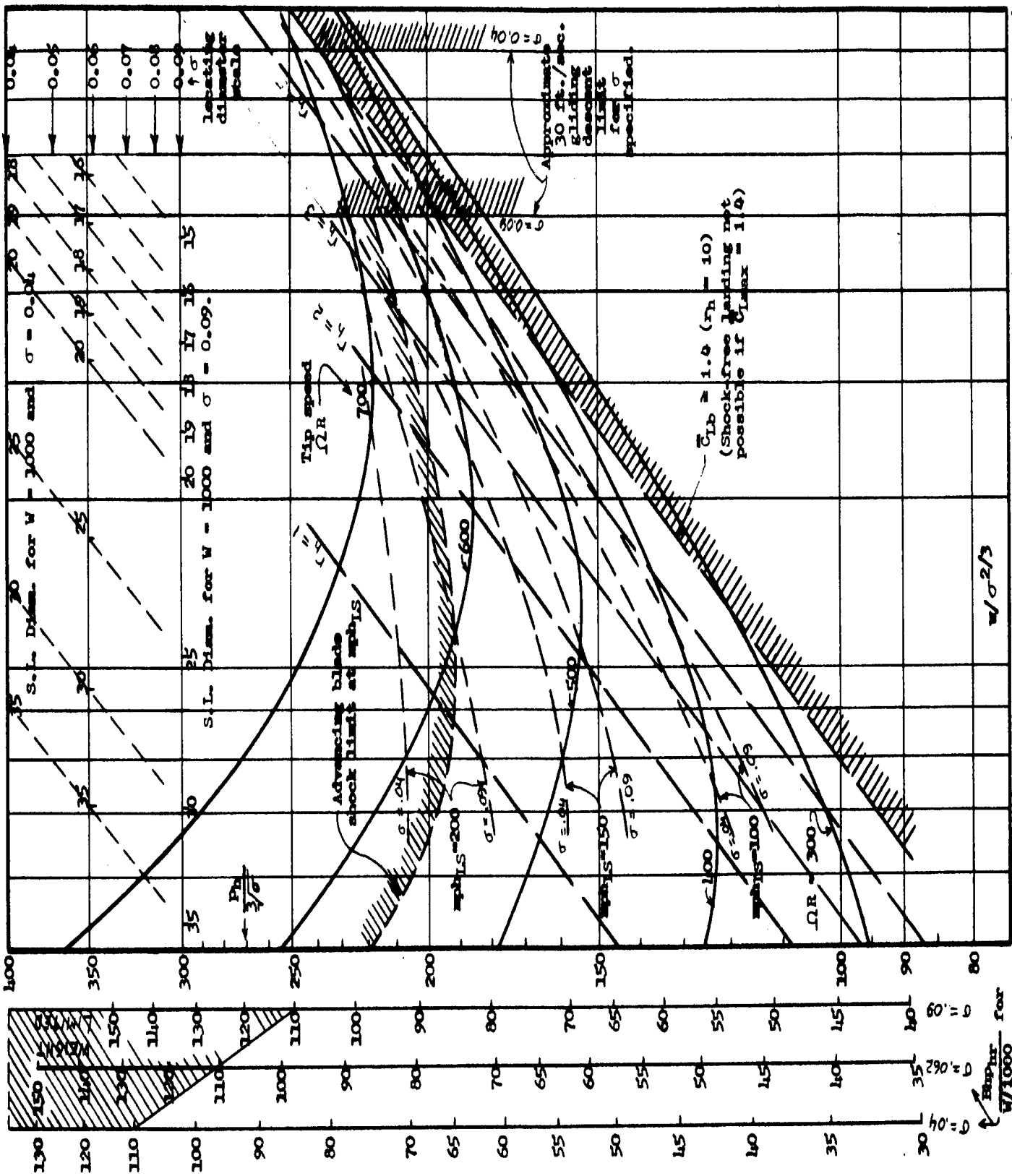


Figure 7. Hovering Power Chart Based on Three-Blade Tower Test Data.

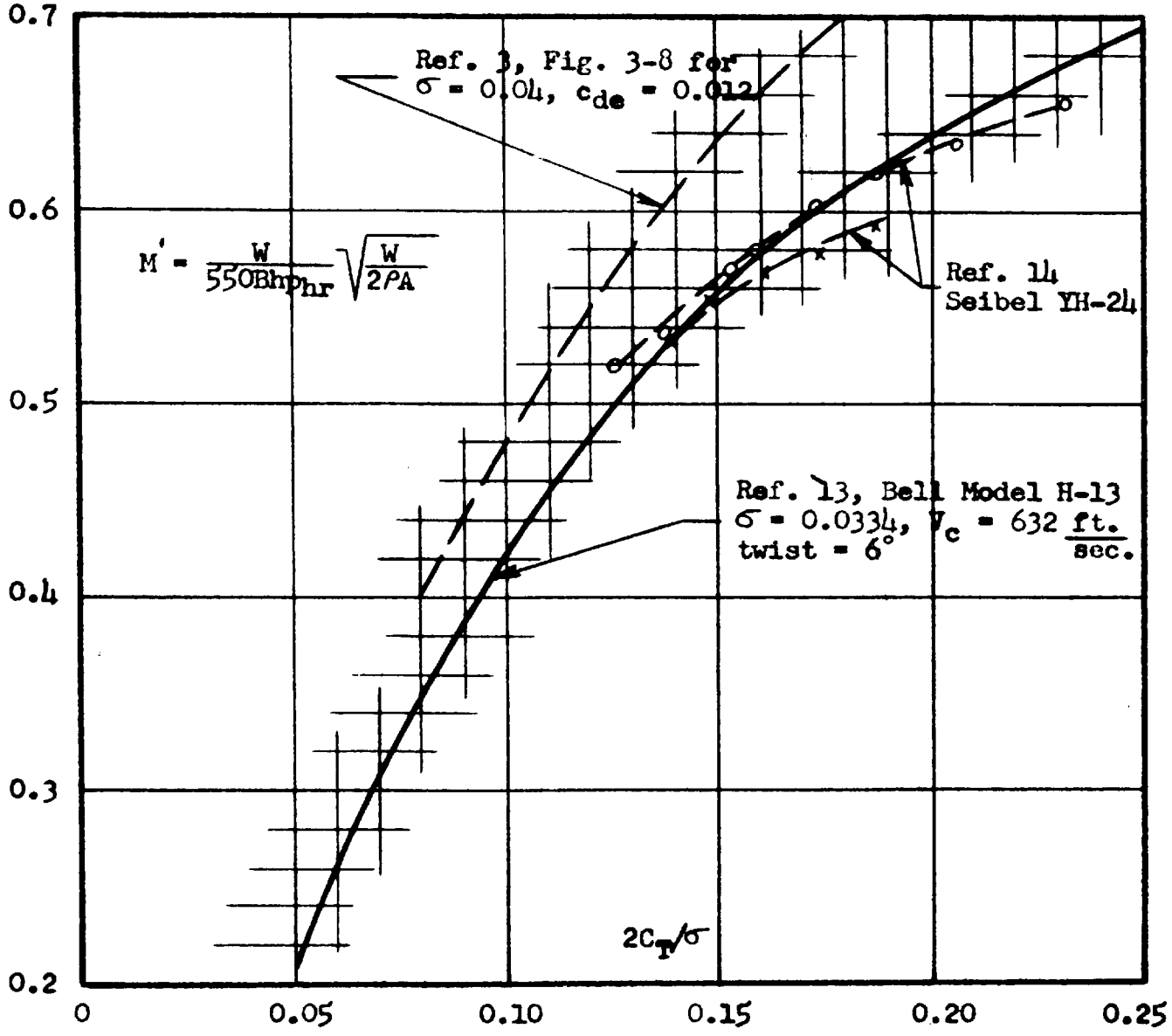


Figure 8. Rotor Figure of Merit for Bell and Seibel Helicopters

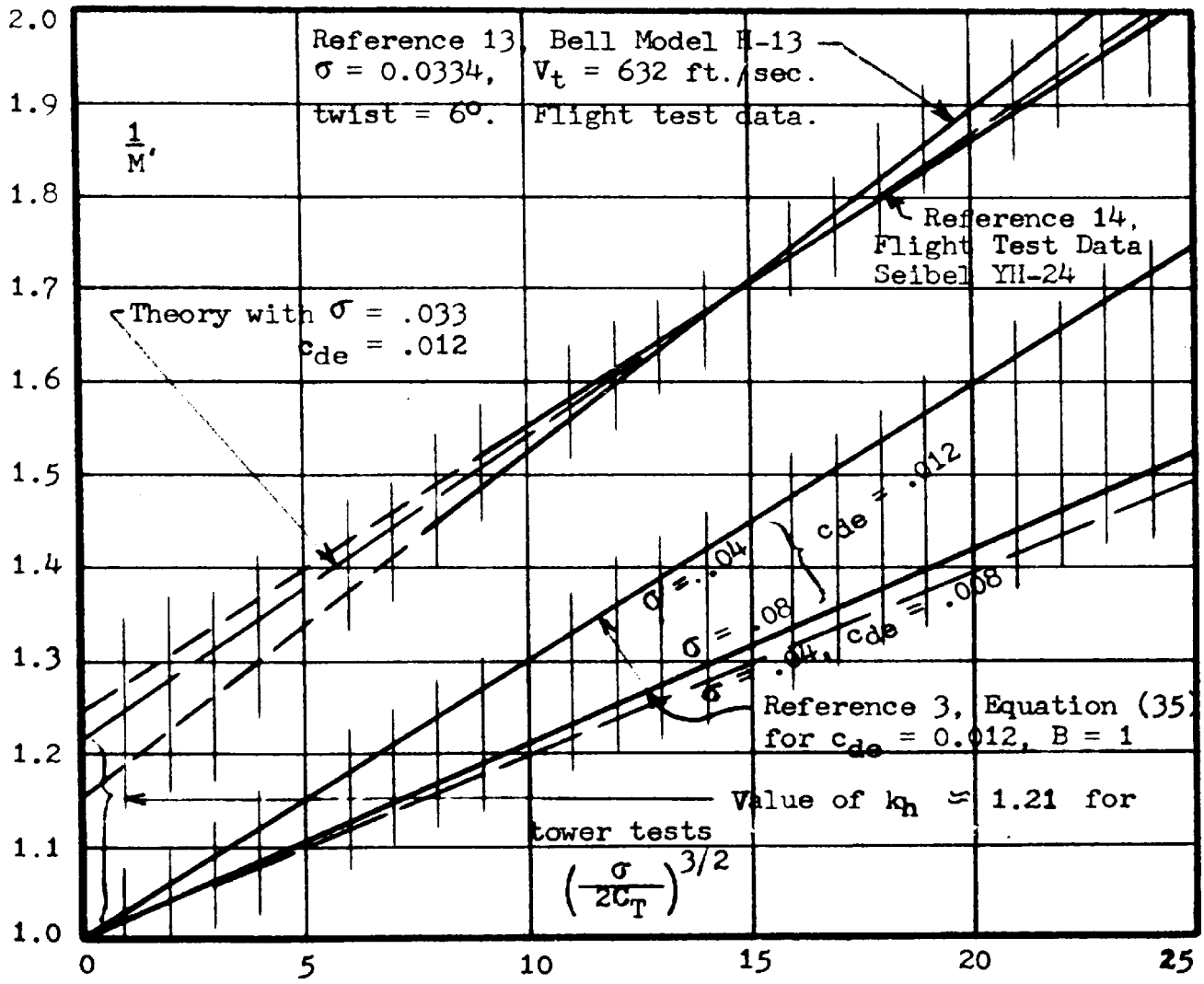


Figure 9.. Reciprocal Figure of Merit Plotted vs. $(\sigma/2C_T)^{3/2}$ for Comparison of Flight Tests and Theory.

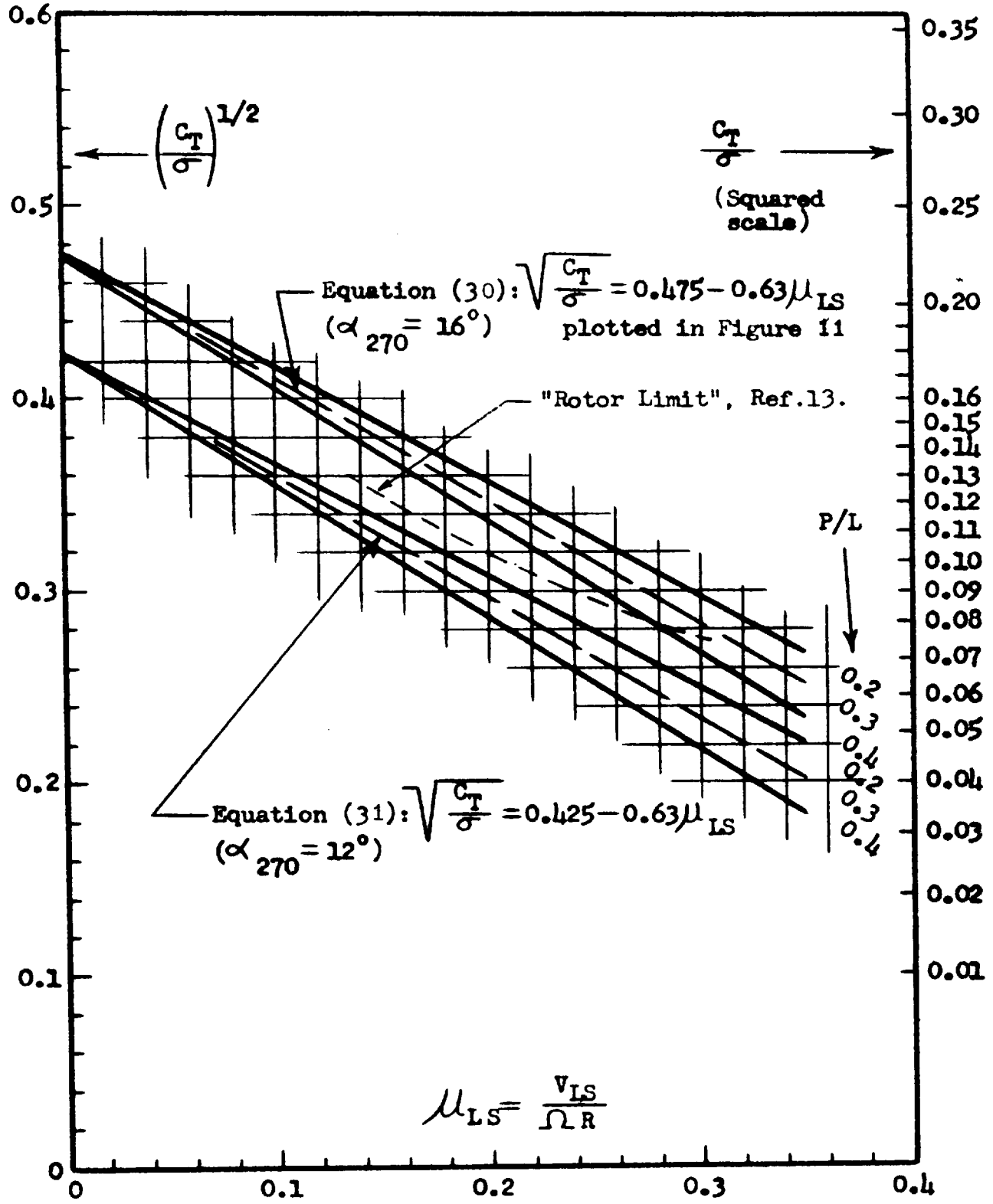


Figure 10. Summary of Retreating Blade Stall Limitations

Solid lines from Figures 10-10 and 10-11, reference 3, based on theory and some tests.

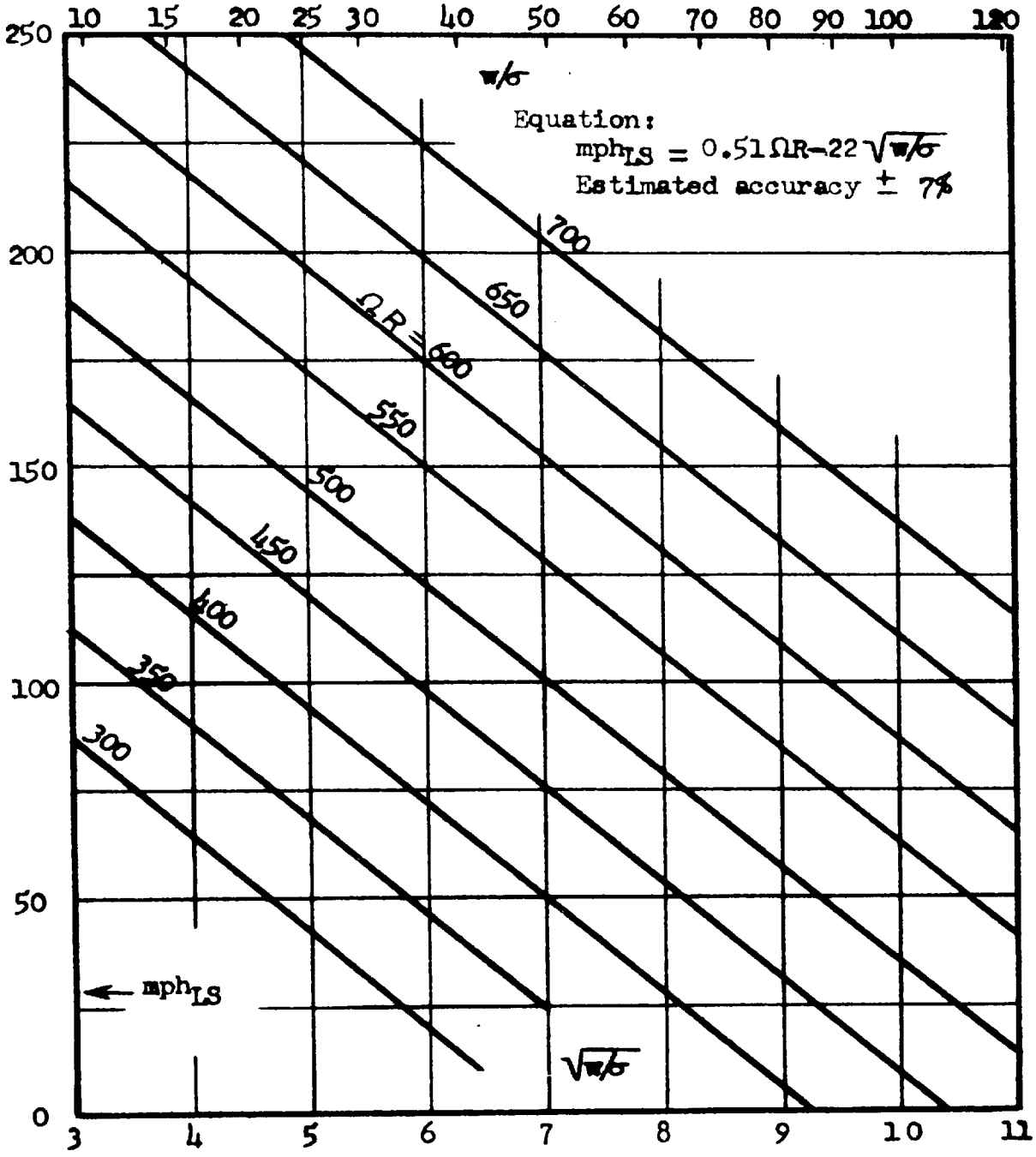


Figure 11. Plot of Retreating Blade Stall Limitations Based on Figure 10.

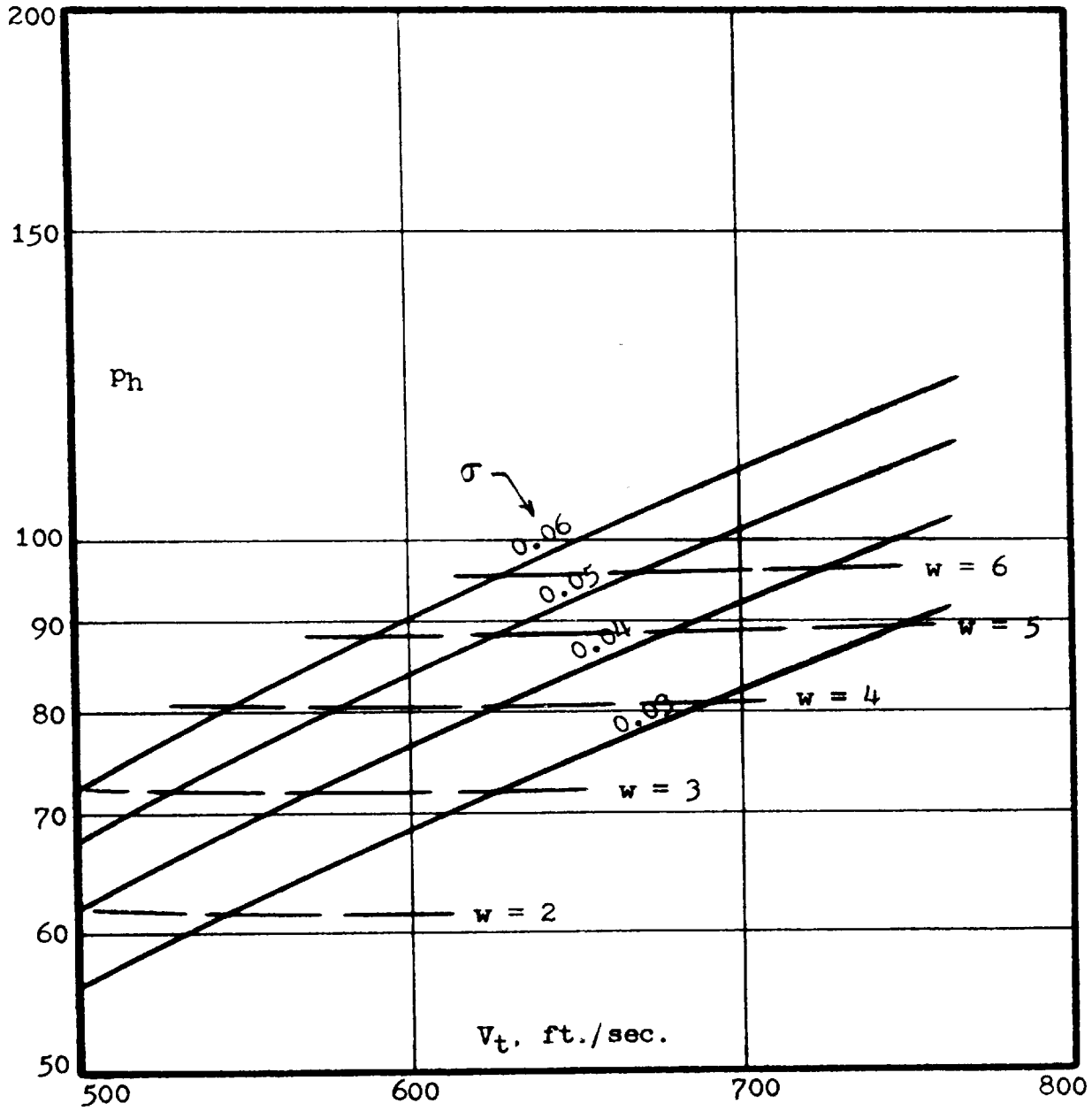


Figure 12. Hovering Power per 1000 Pounds Gross Weight Plotted vs. V_t With w and σ as Parameters for a Constant Rotor Limit of mph_{LS} = 100.

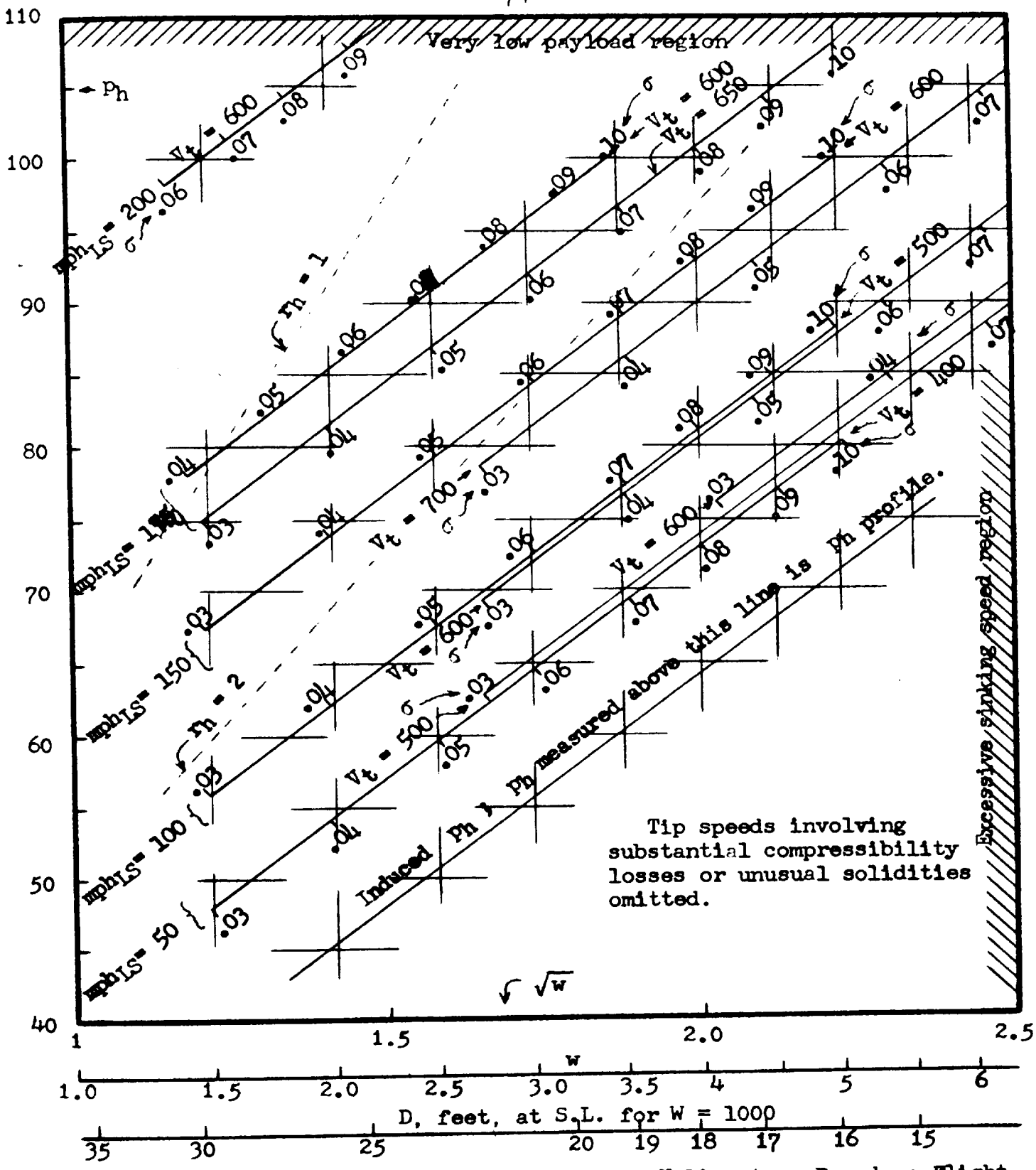


Figure 13. Hovering Power Chart for Two-blade Helicopters Based on Flight Test Data in Figure 9.

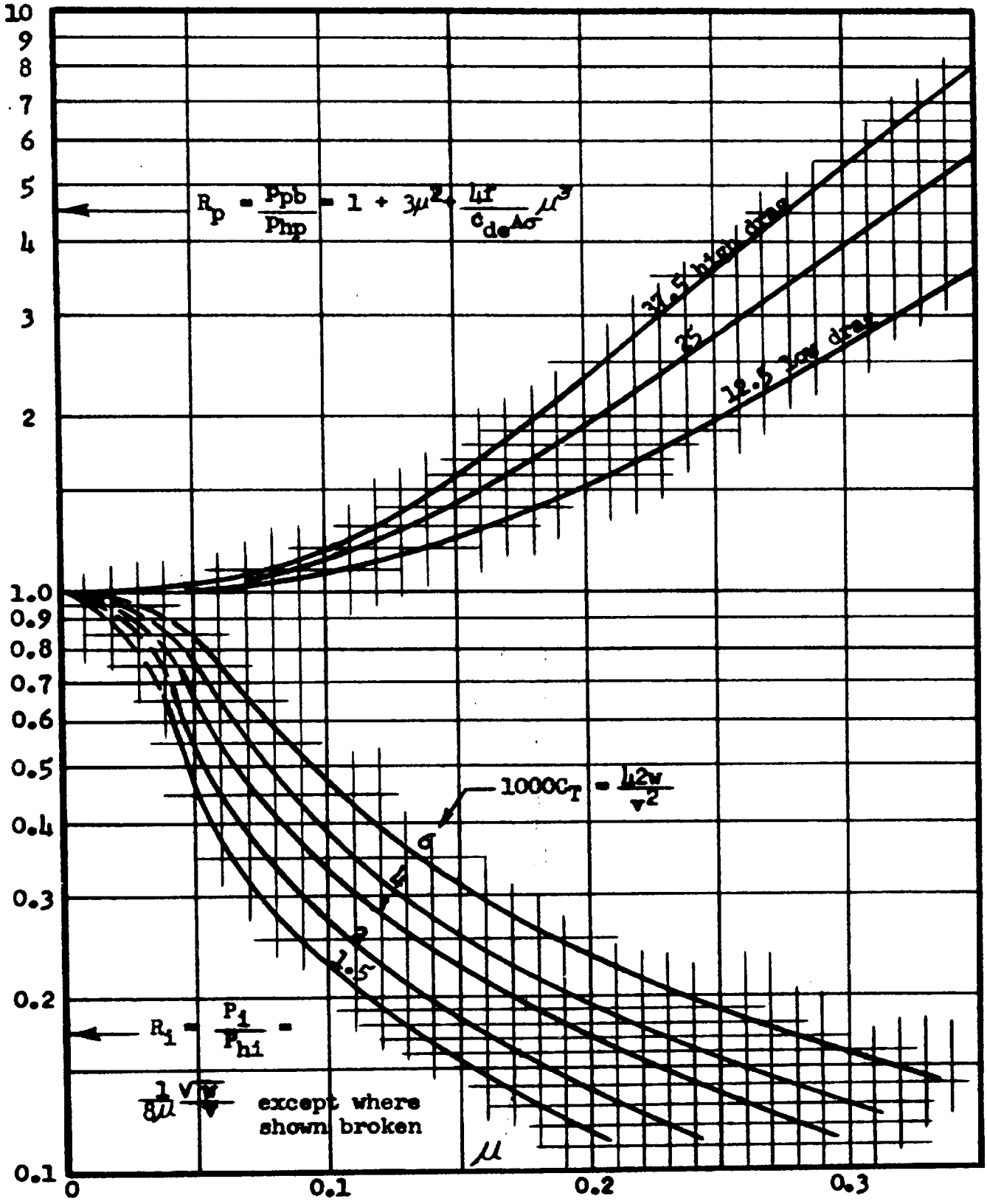


Figure 14. Variation of Induced and (Profile + Body) Power with Speed Ratio.

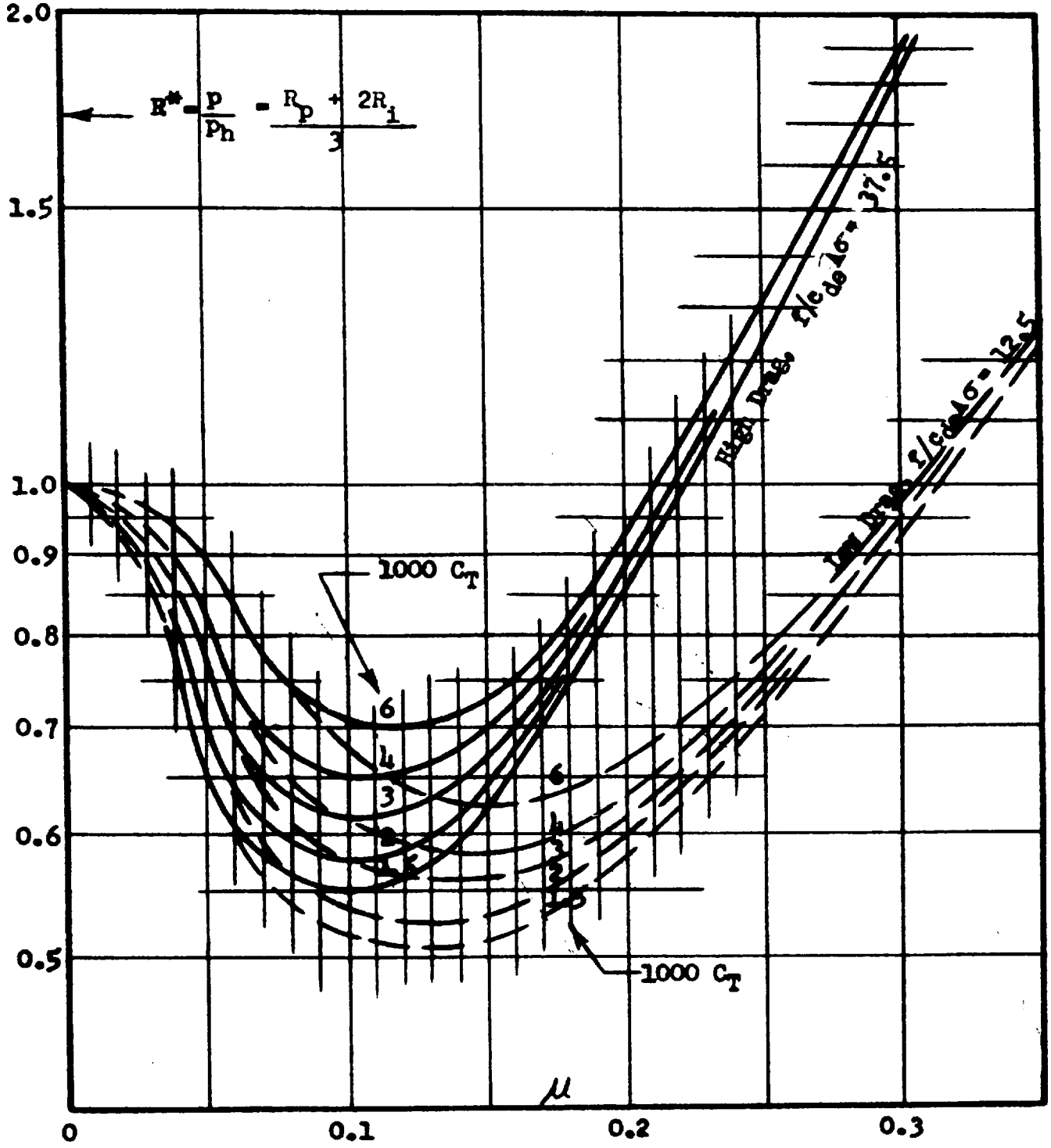


Figure 15. General Power Required Chart for Level Flight of Optimum Helicopters ($\eta_h = p_{hi}/p_{hp} = 2$).

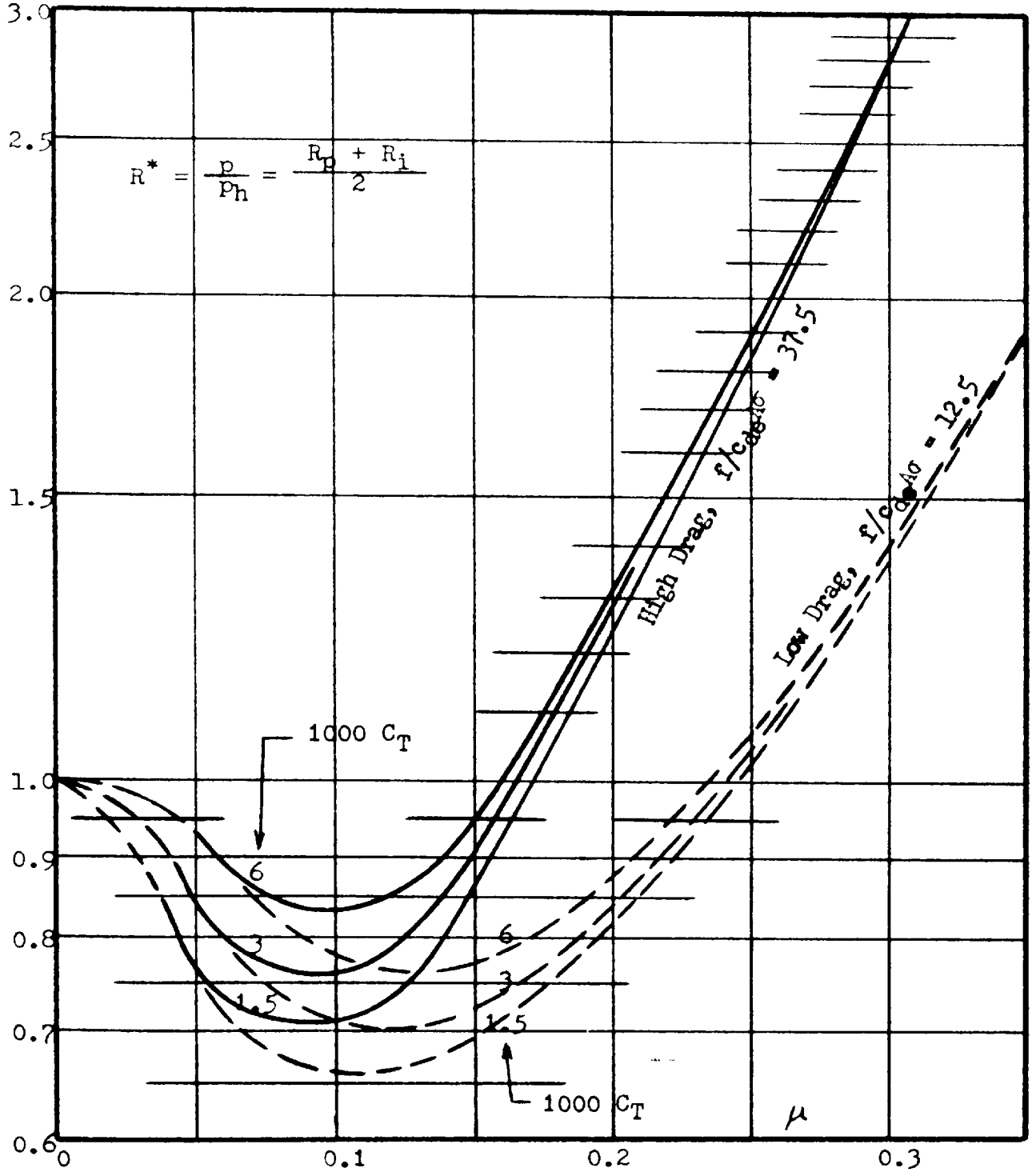


Figure 16. General Power Required Chart for $r_h = 1$.

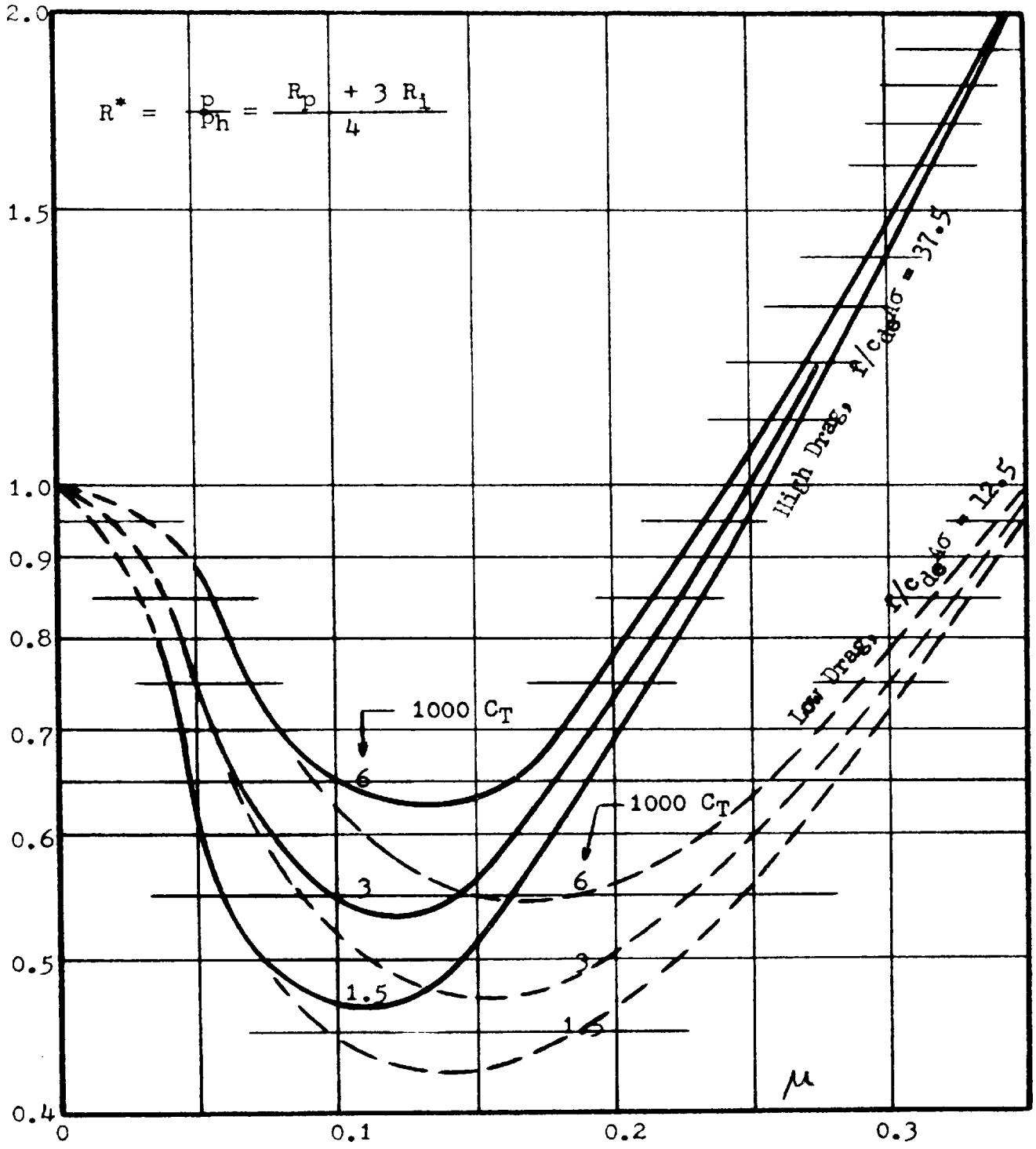


Figure 17. General Power Required Chart for $r_h = 3$.

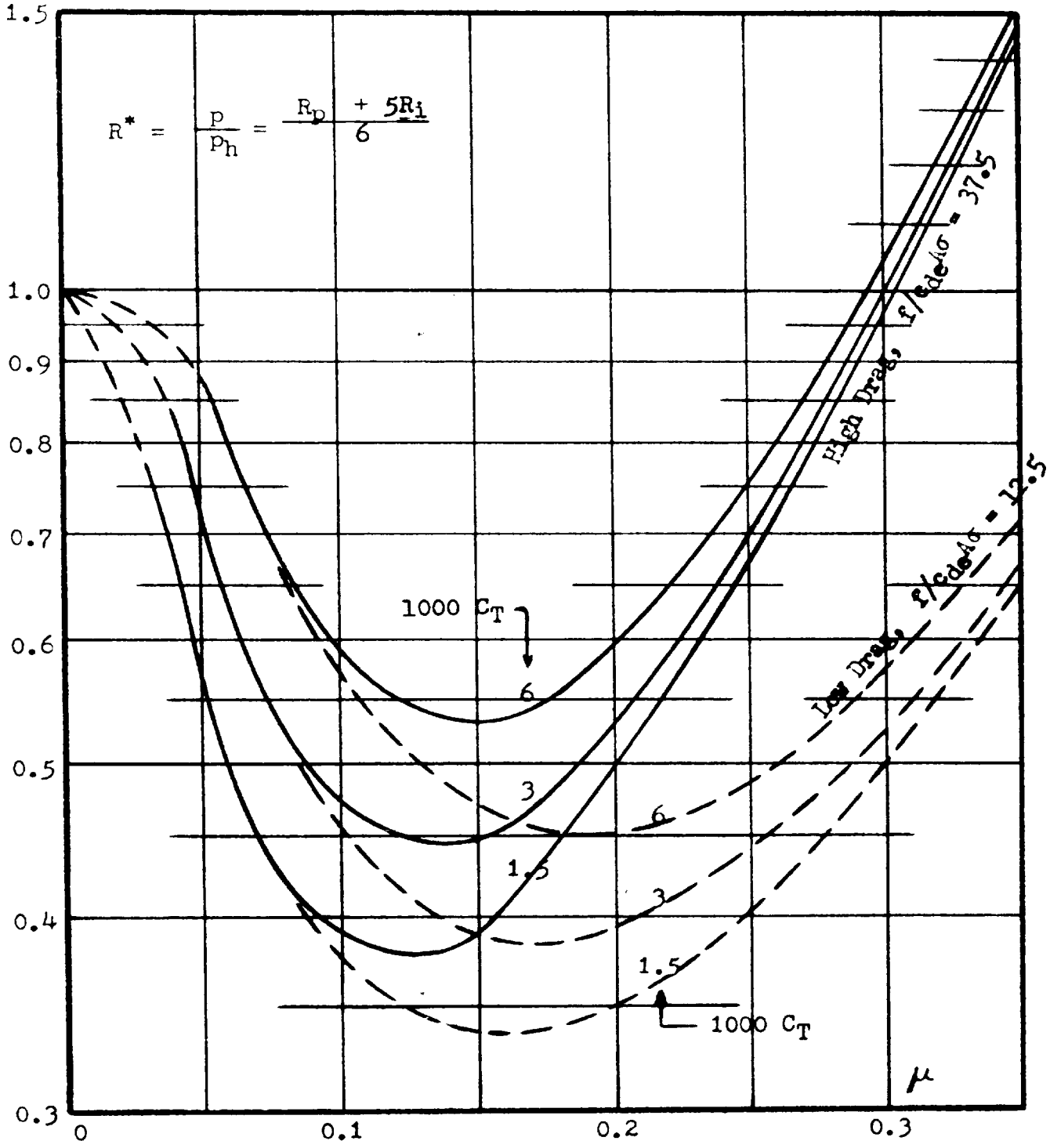


Figure 18. General Power Required Chart for $r_h = 5$.

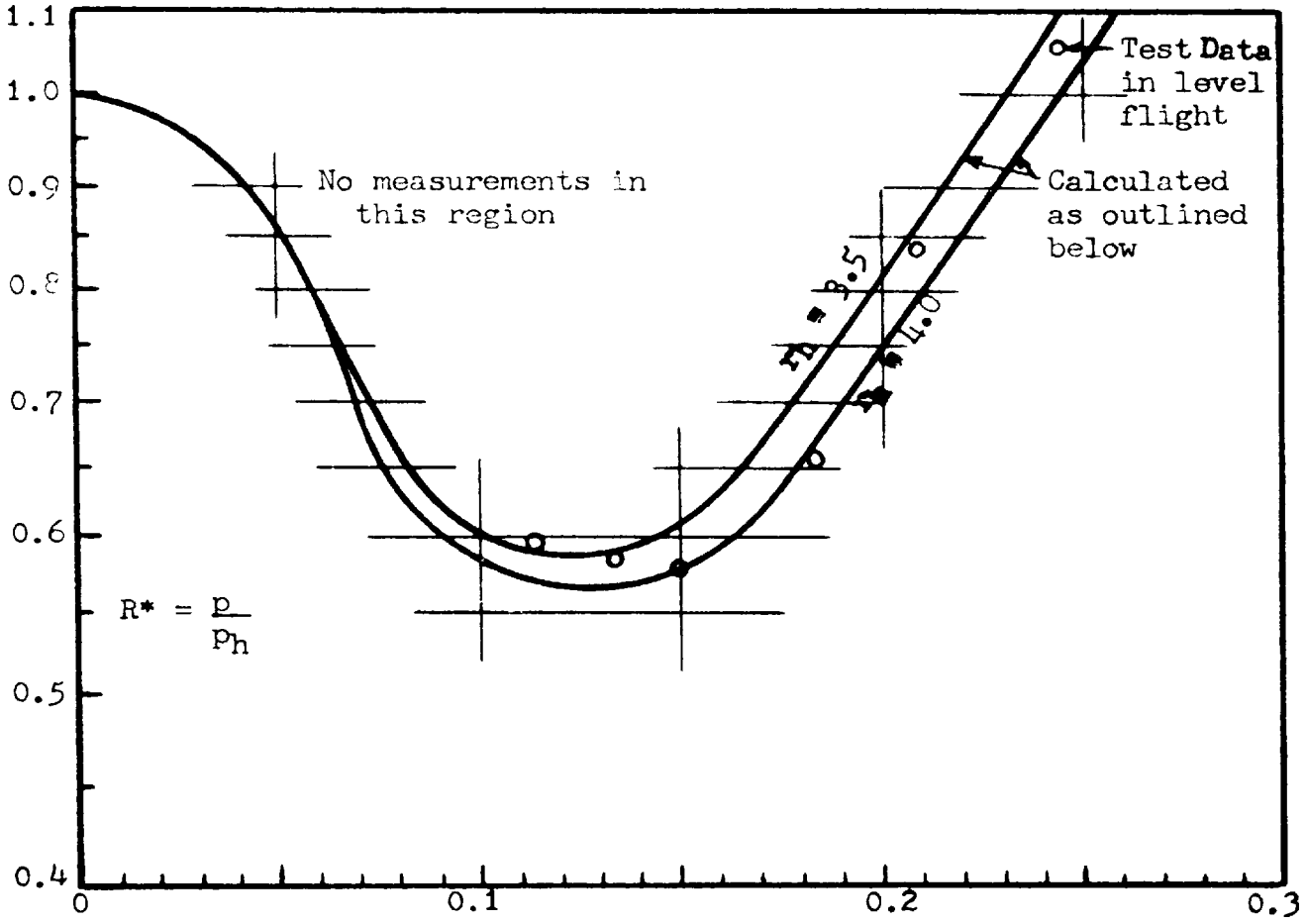


Figure 19. Flight Test Check on General Power Required Chart.

Test data on Sikorsky Helicopter Model HNS-1 from NACA TN 1595. Measured $f/A\sigma = 0.375$ without rotors. Estimated $f/A\sigma = 0.40$ including rotor hub. Estimated $f/c_{de}A\sigma = 50$ (if $c_{de} = 0.008$). Measured $w = 2.58$; measured $w/\sigma = 62$; measured $\sigma = 0.042$. Measured $p_h = 54 \pm 1$ horsepower per 1000 pounds gross weight at $v = 4.5$ to 4.8. Measured average $1000C_T = 4.6 \pm 0.7$.

Calculated $1000C_{T_h} = 4.7$ to 5.3 from measurements.
Calculated $p_{hi} = 10.8$, $p_{hp} = 54 - 10.8 = 43.2$; $r = 4.0$.

Calculated $p_{hp} = \frac{0.014}{0.008} 4.32 \frac{v^3}{w/\sigma} = 12$ based on $c_{de} = 0.014$;

$p_{hi} = 54 - 12 = 42$, $r_h = 3.5$.

"Calculated" lines above based on $r_h = 3.5$ and 4, $f/c_{de}A\sigma = 50$, and $1000C_T = 4.8$, using Figure 14, as follows:

						Notes below.
μ	=	.05	.10	.15	.20	.25	
R_i	=	.80	.42	.28	.21	.17	(for $1000C_T = 4.8$)
R_p	=	1.08	1.22	1.75	2.90	4.50	(for $f/c_{de}A\sigma = 50$)
$R_1^* = \frac{R_p + 4R_i}{5}$	=	.86	.58	.57	.75	1.04	(for $r_h = 4.0$)
$R_2^* = \frac{R_p + 3.5\,R_i}{4.5}$	=	.86	.60	.61	.81	1.14	(for $r_h = 3.5$)

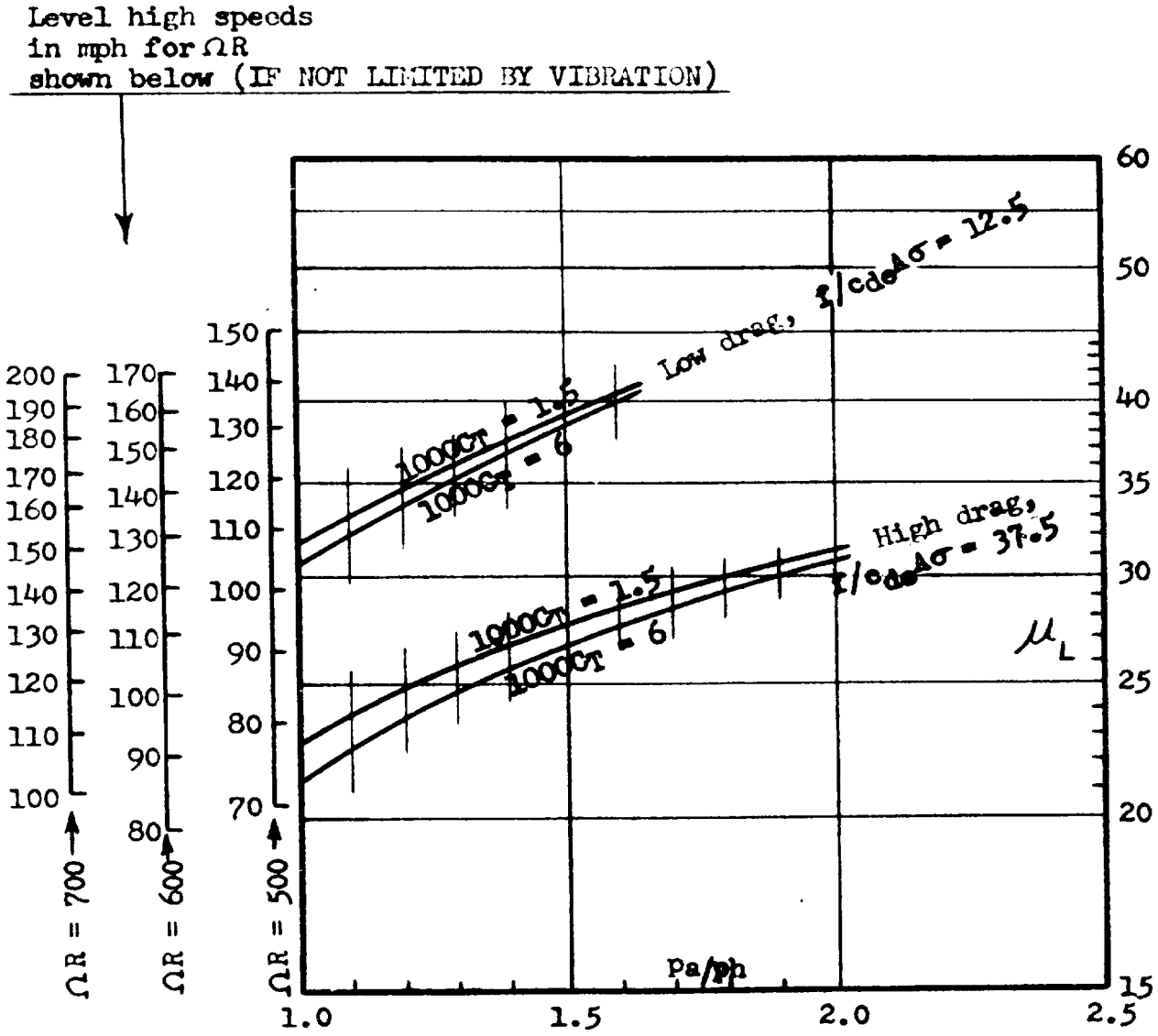


Figure 20. Sea Level High Speed Chart for Optimum Designed Helicopters with $n_h = P_{hi}/P_{hp} = 2$

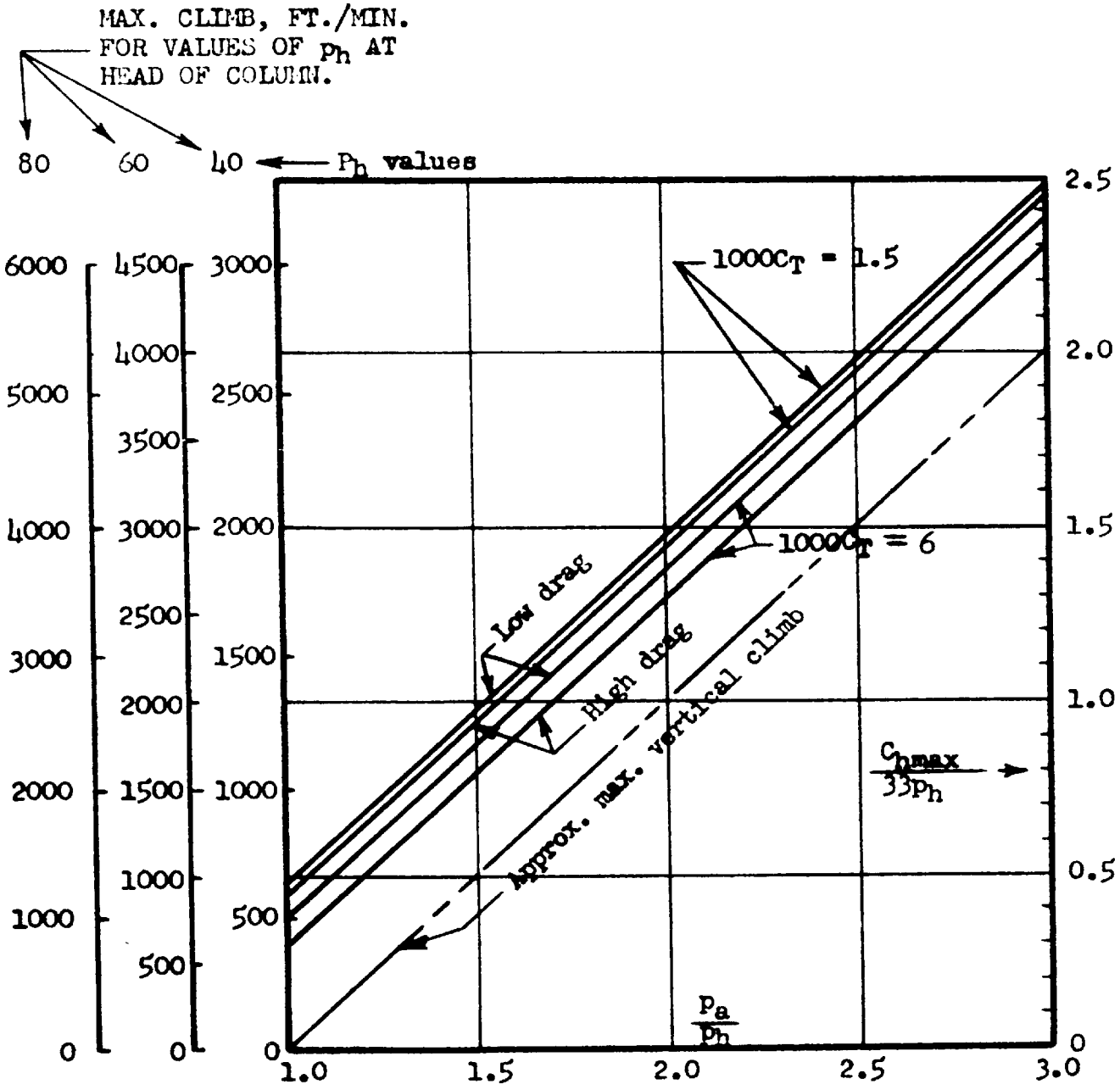
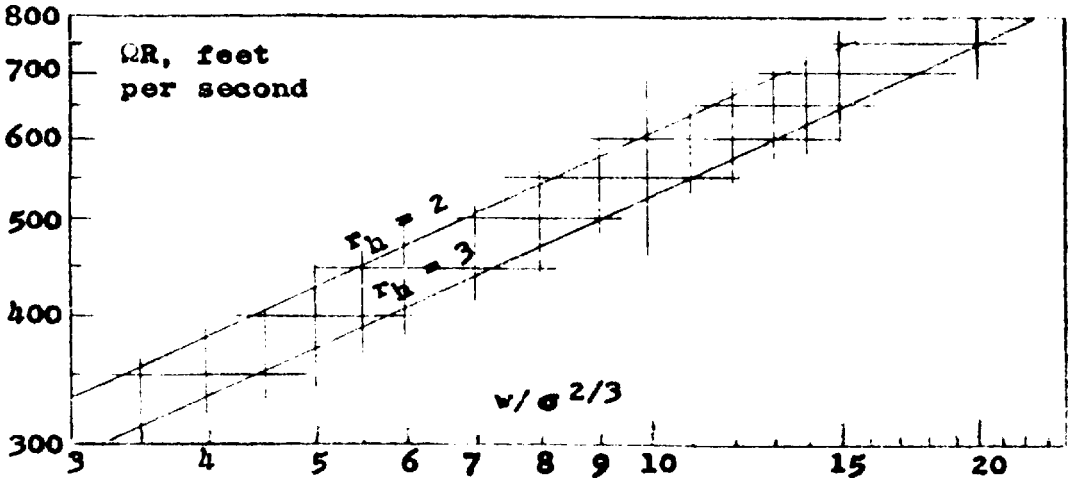


Figure 21. Maximum Sea Level Climb Chart for Optimum Designed Helicopters with $r_h = P_{hi}/P_{hp} = 2$



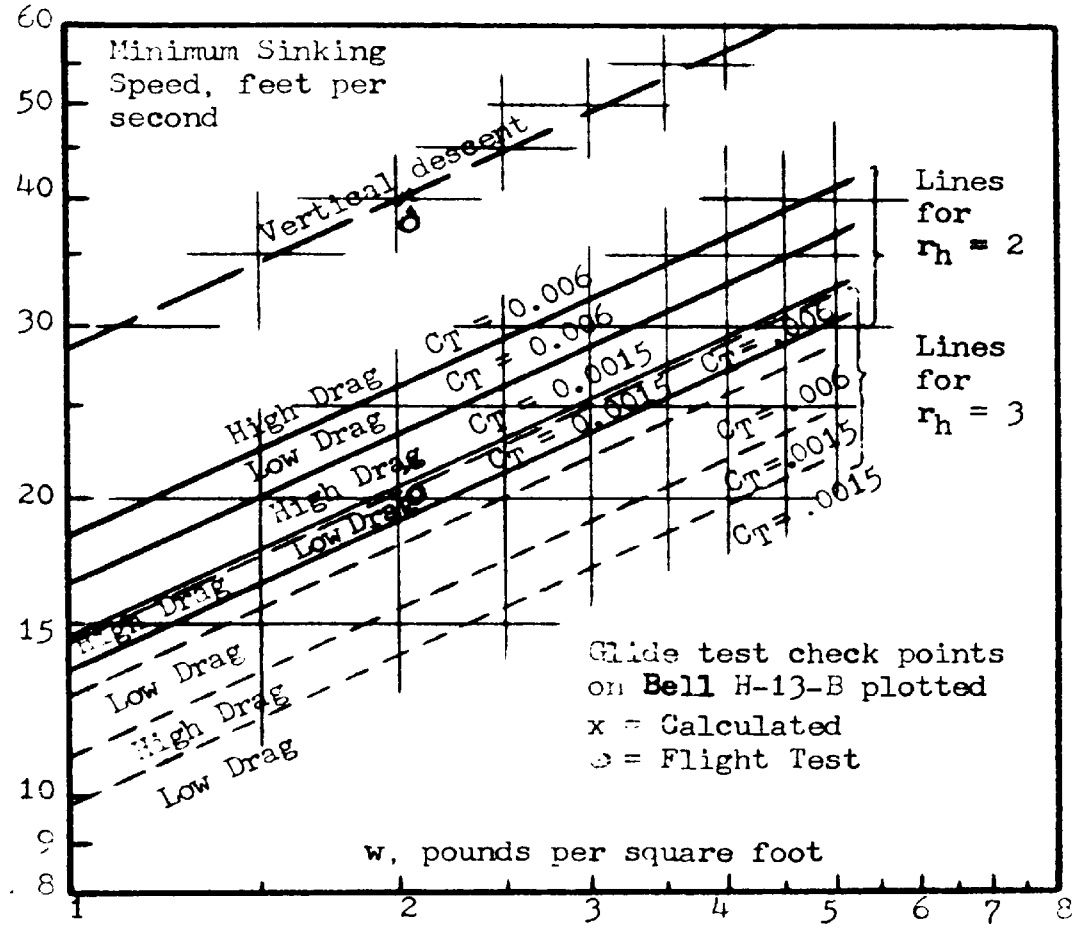


Figure 22. Simplified Approximate Calculated Sinking Speed of Helicopters in Autorotative Descent at the Rotative Speeds Specified Above.

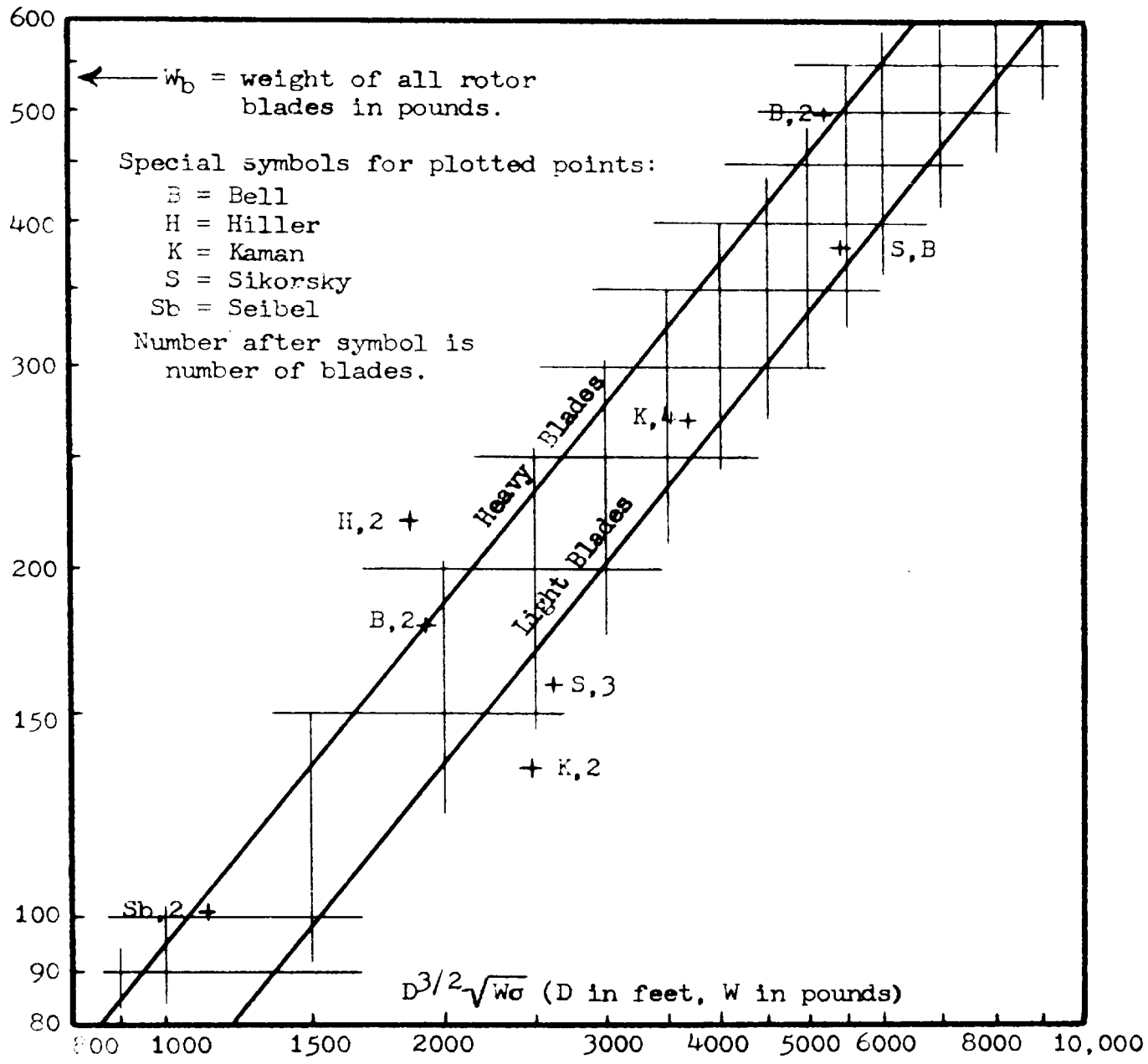


Figure 23. Plot of Some Rotor Blade Weights, Based on Data in Reference 1.